7-18-2018

# An Assessment of Small Unmanned Aerial Systems in Support of Sustainable Forestry Management Initiatives

Michael P. McClelland II
mpm2408@rit.edu

# An Assessment of Small Unmanned Aerial Systems in Support of Sustainable Forestry Management Initiatives

by

Michael P. McClelland II

A.S. Northern Virginia Community College, 2009

B.S. George Mason University, 2012

A thesis submitted in partial fulfillment of the

requirements for the degree of Master of Science

in the Chester F. Carlson Center for Imaging Science

College of Science

Rochester Institute of Technology

July 18, 2018

Signature of the Author _____

Accepted by _____

Coordinator, M.S. Degree Program Date

CHESTER F. CARLSON CENTER FOR IMAGING SCIENCE

COLLEGE OF SCIENCE

ROCHESTER INSTITUTE OF TECHNOLOGY

ROCHESTER, NEW YORK

CERTIFICATE OF APPROVAL

---

M.S. DEGREE THESIS

---

The M.S. Degree Thesis of Michael P. McClelland II
has been examined and approved by the
thesis committee as satisfactory for the
thesis required for the
M.S. degree in Imaging Science

---

Dr. Jan van Aardt
Thesis Advisor

---

Dr. Carl Salvaggio
Committee Member

---

Dr. Emmett Ientilucci
Committee Member

---

Date

**An Assessment of Small Unmanned Aerial Systems in Support of Sustainable Forestry Management Initiatives**

by

Michael P. McClelland II

Submitted to the
Chester F. Carlson Center for Imaging Science
in partial fulfillment of the requirements
for the Master of Science Degree
at the Rochester Institute of Technology

## Abstract

Sustainable forest management practices are receiving renewed attention in the growing effort to make efficient long-term use of natural resources. Sustainable management approaches require accurate and timely measurement of the world's forests to monitor volume, biomass, and changes in sequestered carbon. It is in this context that remote sensing technologies, which possess the capability to rapidly capture structural data of entire forests, have become a key research area. Laser scanning systems, also known as lidar (light detection and ranging), have reached a maturity level where they may be considered a standard data source for structural measurements of forests; however, airborne lidar mounted on manned aircraft can be cost-prohibitive. The increasing performance capabilities and reduction of cost associated with small unmanned aerial systems (sUAS), coupled with the decreasing size and mass of lidar sensors, provide the potential for a cost-effective alternative. Our objectives for this study were to assess the extensibility of established airborne lidar algorithms to sUAS data and to evaluate the use of more cost-effective structure-from-motion (SfM) point cloud generation techniques from imagery obtained by the sUAS. A data collection was completed by both manned and sUAS lidar and imaging systems in Lebanon, VA and Asheville, NC. Both systems produced adequately dense point clouds with the manned system exceeding 30 pts/$m^2$ and the sUAS exceeding 400 pts/$m^2$. A cost analysis, two carbon models and a harvest detection algorithm were explored to test performance. It was found that the sUAS performed similarly on one of the two biomass models, while being competitive at a cost of $8.12/acre, compared to the manned aircraft's cost

of $8.09/acre, excluding mobilization costs of the manned system. On the biomass modeling front, the sUAS effort did not include enough data for training the second model or classifier, due to a lack of samples from data corruption. However, a proxy data set was generated from the manned aircraft, with similar results to the full resolution data, which then was compared to the sUAS data from four overlapping plots. This comparison showed good agreement between the systems when ingested into the trained airborne platform's data model (RMSE = 1.77 Mg/ha). Producer's accuracy, User's accuracy, and the Kappa statistic for detection of harvested plots were 94.1%, 92.2% and 89.8%, respectively. A leave-one-out and holdout cross validation scheme was used to train and test the classifier, using 1000 iterations, with the mean values over all trials presented in this study. In the context of an investigative study, this classifier showed that the detection of harvested and non-harvested forest is possible with simple metrics derived from the vertical structure of the forest. Due to the closed nature of the forest canopy, the SfM data did not contain many ground returns, and thus, was not able to match the airborne lidar's performance. It did, however, provide fine detail of the forest canopy from the sUAS platform. Overall, we concluded that sUAS is a viable alternative to airborne manned sensing platforms for fine-scale, local forest assessments, but there is a level of system maturity that needs to be attained for larger area applications.

## Acknowledgments

I would like to thank my wife, Kristen, for the patience she has shown as I have progressed through this degree program while living in two separate states and the non-stop support she has given me. She is much stronger than I. Thank you to my immediate family for pushing me to strive for improvement in all that I do. I would never had made it to, and through this program without their support. My Air Force family deserves thanks for all of the mentoring and assistance they have given me in my short career thus far. Notable members that helped keep me pointed in the right direction are Lieutenant Colonel Laura Robinson, Lieutenant Colonel Matthew Holston, Lieutenant Colonel Konstantin Sverkounov, Captain Marc Luek, Captain Kyle Clements, Captain Orlando Martinez, and Captain Ben Deschane. Thank you, Dr. van Aardt, for the guidance and wisdom shared with me throughout the research process in regards to science and life in general. Thank you to all of the professors in the Center that taught the courses enabling me to perform quality scientific research. Of these professors, I would like to specifically thank Dr. Charles Bachmann for the patience shown during radiometry while I tried to shake off four years of rust on my calculus skills and Dr. Chris Kannan for teaching the most useful programming class I have taken in my academic career. Lastly, I would like to thank the group of students who battled with me through the daunting first year: Tyler Peery, Keegan McCoy, Chris Lapszynski, Baabak Mamaghani, Margot Accettura, and Tyler Hayes. Oh yeah, thanks Eon, one more week!

# Contents

# List of Figures

*LIST OF FIGURES*

# List of Tables

# Chapter 1

# Introduction

## 1.1 CONTEXT

Timber products have supported civilizations for thousands of years, from firewood for heat and cooking, to building materials for shelter and transportation, down to simple paper products for communication in the modern age. A majority of the population rely on products derived from forests, along with the ecosystems and associated services that these forests support. With this in mind, an effort to conserve natural resources is paramount in order to continue associated ecosystem services. However, quantifiable information on forest structure and condition must be collected in order to achieve this goal. Production information, and the communication flow of said information to stakeholders, is a key product within forestry management [1]. This concept was noted over 25 years ago and has become increasingly important today, leading to the need for robust forest measurement techniques. These measurements serve as input to standardized decision-making metrics used by foresters when applying sustainable forest management (SFM) principles.

Historically, measurements have been completed exclusively by ground crews, who manually measure individual stems in representative plots located throughout the entire forest

[2]. From these representative plots, the descriptive forest area measurements can be estimated through the process of imputation [3], which implies a process of filling in data points that were not directly measured. This can be done through various methods, with regression modeling being commonly used in the context of forestry [4]. As expected, it can be tedious and time consuming to deploy a field crew to measure individual trees in forests covering large areas. This does not support rapid acquisition of information, since field inventories can take months to complete. It becomes increasingly difficult, time consuming, and expensive in rugged, mountainous terrain that is difficult to traverse.

Remote sensing technology possesses the capability to execute these measurements in rugged, hard to navigate terrain, while also allowing for large area coverage. Forestry mapping and measurement utilizing remote sensing techniques therefore has become a key research area. Initial studies focused on multi- and hyper-spectral imaging, as well as synthetic aperture radar (SAR) [5]–[8]. The optical imagers suffered insensitivity to above ground biomass (AGB) values of secondary forests beyond 10-15 years of age [9], [10]. Models generated from SAR backscatter returns in turn suffered from similar saturation issues, causing insensitivity to dense forests with AGB values about 60 Mg/ha [5], [6]. These issues made it challenging to rely on remote sensing methods for forestry use, as information for all types of forests are required to inform decision making in the context of sustainable forest management. However, lidar (light detection and ranging) is a relatively novel technology that has shown much promise for forest structural assessment.

Lidar is an active imaging technology that can directly measure structural information of the forests, including forest canopy structure. With the advancement of laser pulse rates and scanning rates, as well as the capability to measure multiple returns per pulse, lidar sensors are capable of generating dense point cloud measurements of the dominant and underlying canopy in mixed aged forests. Many of the parameters that foresters are interested in, such as volume, biomass, and carbon, are modeled through allometric equations that are functions of structural measurements, e.g., diameter at breast height (DBH), core stem height, total height, crown area etc. Airborne lidar scanner (ALS) systems provide a capability to directly measure many of these independent variables used for modeling forestry parameters and for coverage of large areas in relatively short time periods. A variety of studies at plot- and individual tree level successfully have been completed using ALS systems in a variety of forest types and locations, measuring

important SFM metrics, such as volume, biomass, and stems-per-hectare (SPHA) [11]–[14]. This work recently has been extended to the assessment of forest sustainability.

Multiple organizations have been established to develop best practices and methods in regards to sustainable forestry. The UN Framework Convention on Climate Change (UNFCCC) developed an initiative called "Reducing Emissions from Deforestation and Degradation" (REDD+). The initiative requires large-area biomass and carbon inventories to be measured, and incentivizes the concept of carbon credits to offset less environmentally friendly industries, such as power plants [15]. In another international example, the 12 host nations that manage 49% of the world's forest by area, which contain 90% of the world's temperate and boreal forests, follow the Montreal Process for SFM [16]. This process establishes seven criteria as guiding principles, each containing measurable indicators to determine success or failure in maintaining the guidelines at the regional and national scales. These commitments to conservation and SFM principles appear to be effective, as recent trends show total forest area loss has been slowing. For example, forest area loss during the time period from 2010 to 2015 exhibited half the loss rate as seen between 1990 to 2000 [17]. Both of these SFM frameworks require accurate, recurring measurements of forests for monitoring changes in biomass, carbon, and forest structure. These SFM principles drive a need to accurately capture inventory metrics across large areas and to do so in an efficient manner [4], as change detection requires repeated measurement.

The current standard for obtaining ALS data for an area of interest is to contract a company specializing in deploying ALS systems on fixed wing aircraft. Maintaining and operating these systems is an expensive endeavor, and as such, the cost is passed along to the end-user. Studies comparing costs between ground crews manually measuring plot inventories and these airborne scanning systems found that the ALS collections typically cost tens of thousands of US dollars more than a standard ground crew-based collection [2], [3]. The tradeoff, however, is that ALS systems can cover a much larger land area and directly measure entire forests, while the ground crews will measure representative plots and use models to develop estimates for entire forests. Once area is considered, at small area sizes, the ground crew option is more cost effective as mobilization costs outweigh the operation costs of the ALS small area collections. Therefore, as the study area increases, the ALS option becomes more competitive and surpasses the ground crew method in cost [3].

In recent years the reduction in sensor size and mass, coupled with increasing payload capability and flight times of small unmanned aerial systems (sUAS), have provided the opportunity for a third option. This option allows for high operational flexibility at a potentially reduced cost from the typical ALS system deployment. The sUAS is lightweight with a small logistical footprint; there are no recurring fuel costs, and such systems only require a Federal Aviation Administration (FAA) part 107 certified pilot. It is with these benefits in mind that we executed a study to assess sUAS capabilities for forest structural assessment. We hypothesize that with a sUAS, an organization can obtain the same level of accuracy of the legacy ALS systems and can procure higher density point clouds for use in SFM metric analysis, while simultaneously generating adequate imagery (ground sample distance < 10 cm) for fine scale structure-from-motion

The research conducted in this thesis aimed to support these goals of rapid, accurate acquisition of data for use with sustainable forest management practices. Methodologies employed for data collection were manned and sUAS airborne lidar scanning systems, as well as imagery collections completed coincidentally with the lidar collections. The specific objectives of the research conducted are listed in the next section.

## 1.2 OBJECTIVES

- Objective 1: Assess the extensibility of light detection and ranging (lidar) algorithms for forest height, volume, and carbon assessment to sUAS platforms and data.
- Objective 2: Evaluate the use of more cost-effective imagery-based (stereoscopic structure-from-motion) vs. lidar-based algorithms for forest structure assessment.
- Objective 3: Develop and evaluate a framework for disturbance detection within forest canopy structures.
- Objective 4: Publish and present research findings to achieve broad industry dissemination, especially among forest management entities such as the Forest Stewardship Council (FSC) and Rainforest Alliance.

## 1.3 THESIS LAYOUT

### 1.3.1 Chapter 2: Background

This chapter provides a more in depth background of the history of remote sensing in the forestry domain. Basic terms and methods are identified in more detail than what would be found in subsequent chapters.

### 1.3.2 Chapter 3: Cost Analysis Between Sensor Platforms

This chapter contains a paper that was presented and published in the SPIE Commercial and Scientific Sensing and Imaging conference, April 2018 [18]. A simple linear regression model, based on point cloud distributions, is introduced to show that the sUAS and commercial lidar system perform similarly. A cost analysis is presented to compare economic implications of deploying either system for a typical user. Objectives 1 and 4 are addressed by this paper.

### 1.3.3 Chapter 4: Functional Carbon Models in Broad Leaf Deciduous Forests and Harvested Plot Detection

This chapter introduces a functional carbon model based on canopy height distributions, derived from canopy height models. A comparison is completed between a commercial lidar system and sUAS lidar system, with an additional comparison of data generated utilizing structure-from-motion methods on imagery collected by each platform to generate alternate point clouds. Lastly, a classifier is developed to detect disturbed plots and flag potential harvesting. This chapter is written with the intent to submit the study to a peer-reviewed journal within the 2018 – 2019 timeframe and addresses Objectives 1-3.

### 1.3.3 Chapter 5: Summary

This chapter summarizes the work done at the time of writing, presents the current conclusions and describes future work and improvements to be considered for continuation of the research topics.

## 1.4 SCIENTIFIC CONTRIBUTIONS

- Demonstrated higher point density capability of sUAS systems, capturing greater structural detail of dominant canopies.
- Demonstrated greater capability of sUAS structure-from-motion point clouds to overcome perspective issues encountered with the fixed wing aircraft data.
- Demonstrated the ability of sUAS lidar to detect harvested forest using structural metrics derived from voxels.
- Analyzed economics and compared the quality of products between commercially generated lidar and sUAS platform lidar.
- Application of a functional carbon model in a deciduous forest environment, differing from the original synthetic and coniferous forest training sets (from literature).

These contributions have been presented at as SPIE Commercial + Scientific Sensing and Imaging Conference proceedings, April 2018 (Chapter 3), while Chapter 4 is written with the intent to submit for publication in an applicable remote sensing or forestry focused journal.

# Chapter 2

# Background

## 2.1 FOREWORD

This thesis is organized in the modern format, meaning that each of the primary chapters (Chapter 3 and Chapter 4) is a stand-alone paper, including the standard background section. This additional background chapter is provided as a more in-depth review of lidar basics and sUAS applications within sustainable forest management. This chapter concludes with the RIT sUAS platform specifications and with an in-depth review of the preprocessing steps required to complete analysis that were not appropriate for the formal papers presented in later chapters.

## 2.2 LIDAR BASICS

Lidar is an active sensing technology, meaning that the sensor itself generates the energy used for measurement, as opposed to passive platforms such as electro-optical telescopes, which measure energy emanating for the target scene, regardless of the source of the scene radiation. Lidar emits a laser beam and measures the time delta between detected backscatter pulses. This allows for a distance measurement to be made, since the speed of light is known. This distance measurement can be leveraged to generate a point cloud in three-dimensional space if the

location of the sensor is known and the line of sight from the sensor is known. The general governing equation for lidar range measurements in the airborne laser-scanning environment can be seen in Equation 2.1, as described by *Baltsavias* [19].

$$R = c \cdot \frac{\Delta t}{2} \tag{2.1}$$

where, $R$ is the measured distance or range from the sensor to the imaged target, $c$ is the speed of light in the atmosphere, and $\Delta t$ is the change in time from pulse emission to measured return pulse. The energy covers the distance to the target twice, once to the target from the emitter and once back to the receiver from the target, thus, this time is halved for the range measurement.

If the sensor platform's position and attitude geometry (roll, pitch, and yaw) is known in three-dimensional space, coordinate information can be attributed to each range measurement. This coordinate information can be used to generate a point cloud in local coordinate space or in a known coordinate reference system. Typically, a GPS sensor for global position is used to place the location of the sensor in latitude, longitude and altitude space, while and inertial measurement unit (IMU) is used to measure the attitude of the sensor in the roll, pitch and yaw space. These varying coordinates and look angles are depicted by *McCaughey* in his manual for the FUSION lidar processing software suite [20] and can been seen in Figure 2.1. This method of generating lidar point clouds requires precise and accurate timing to properly place points in their correct location in three-dimensional space; otherwise, the structural measurements will not accurately represent the scene. The clock from the GPS sensor is the most reliable and is generally used to synchronize the timestamps or clock systems of the other two devices, the lidar sensors and IMU.

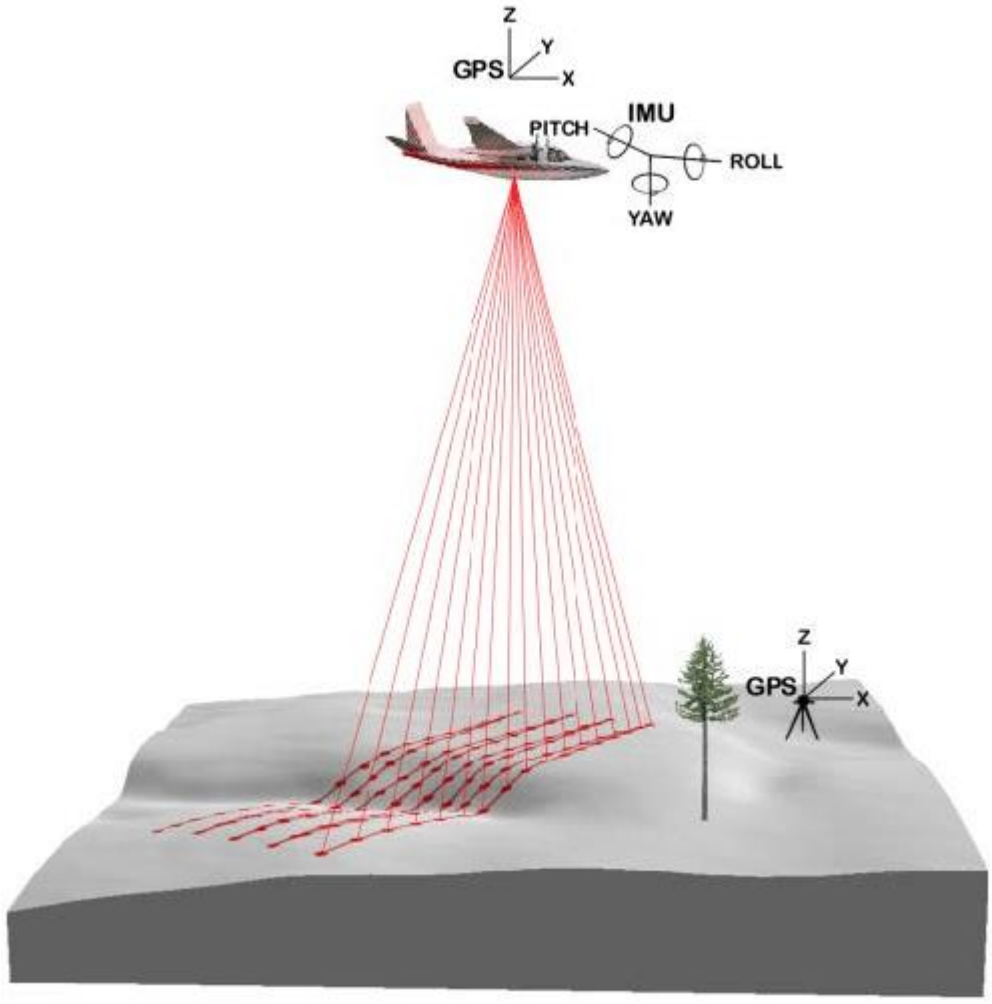


Figure 2.1. An illustration of the varying geometrical properties that influence point cloud generation from airborne laser scanners [20].

## 2.3 sUAS APPLICATIONS

The utility of lidar in the forestry domain has been demonstrated going back over 50 years [21]. The structural measurements made by lidar systems can be used for measurement of many forest characteristics, including biodiversity information, stems per hectare, canopy statistics, biomass estimates, and carbon estimates [11], [12], [14], [22], [23]. The multi-return nature of the lidar system allows for the capture of structural information of heterogeneous and older forest growth that the early remote sensing methods struggled to measure. A hindrance to using airborne laser scanning (ALS), versus the ground crew direct measurement method, is cost

[24], [25]. ALS collections on fixed wing aircraft typically cost tens of thousands of US dollars more than a standard ground crew-based collection, causing difficulty in generating widespread use of the technology [2], [3]. A growing alternative to the commercial fixed wing aircraft approach is the small, unmanned aerial system (sUAS), defined by the Federal Aviation Association as an unmanned aircraft weighing less than 55 lbs at time of takeoff [26].

In recent years, there has been an increase in the use of sUAS for remote sensing of forests [18], [24], [25], [27]–[29]. *Jaakkola et al.* produced one of the earliest sUAS ALS systems for forest management in 2010, after which sUAS use has become more common [24]. This increase in use can be attributed to a few advancements: the increased payload and flight time capability seen with the modern sUAS, a reduction in sensor mass of cameras, lidar systems, and GPS/IMU systems, and an increase in GPS/IMU accuracy in placement of the airframe and characterization of the airframe's attitude during flight (roll, pitch, and yaw). All of these factors allow for larger areas to be imaged, while enabling high quality data products to be generated from these platforms with an ability to fly daily at a low cost of operation [18]. It has been shown that with the higher density point clouds generated from the sUAS, several metrics of interest can be measured with higher precision than larger footprint ALS systems on manned aircraft [24], [30].

There are two common approaches to generating the three-dimensional point cloud products with the sUAS. The first and lower cost solution is the structure-from-motion (SfM) method [31]–[33]. This can be done using a common high spatial resolution RGB camera and acquiring overlapping imagery from multiple viewpoints. Modern software packages have been developed using computer vision algorithms to detect matching points in overlapping images and then use standard photogrammetric methods for height extraction of such a matching point [34], [35]. sUAS systems are well suited to SfM missions, especially rotor type sUAS air frames with vertical takeoff and landing capabilities, as they are capable of capturing hundreds to thousands of images of the target scene with large overlap, 360° coverage, and minimal motion blur. A disadvantage of the SfM methods is that in order to gather a height measurement of a target, it must be in the unobstructed view of the camera from multiple perspectives. A dense, closed canopy presents a significant challenge to this type of measurement as it is difficult to detect enough ground points for height normalization, often leading to a need for an externally sourced digital elevation model (DEM) [24], [25], [34], [36], [37].

The second method is to use a lidar system mounted on the sUAS, with multiple sUAS lidar systems having been explored; in fact, this technology is maturing to be a standard method of forest measurement [24], [25], [27], [30]. This method has an advantage given its ability to measure multiple returns - it can gather much more information about the underlying canopy and terrain than the SfM methods. It has been shown that with the sUAS there is a capability to gather high resolution lidar data (>50 pts/$m^2$), allowing for a more accurate representation of the forest structure to be obtained than a typical manned ALS systems [25], [27]. Generally, the terrain models generated from ALS also are more accurate than those generated from SfM methods [36]. These advantages do come at a higher equipment cost and there is not a standard software for managing lidar point clouds, as there is when generating SfM point clouds. These disadvantages, however, do not outweigh the gains made in data quality provided by the lidar.

## 2.5 CHESTER F. CARLSON CENTER FOR IMAGING SCIENCE sUAS

The airframe used for the sUAS during data collections conducted in Lebanon, VA and Asheville, NC was a DJI Matrice M-600 Pro. This sUAS weighs 10 kg, including batteries, and has a payload capability of 5.5 kg (~ 12.13 lbs). The system is capable of a maximum range from the pilot's location of 5.5 km, before loss of communication with the controller. This range would be difficult to exceed due to the line of sight requirement imposed by the FAA on operations of sUAS, which are defined as systems having a mass less than 55 lbs at time of takeoff [26]. A custom payload support system was designed for integrating a modular sensor platform, allowing for various sensor types and combinations to be flown with the system. This sUAS is capable of hovering at full weight for approximately 18 minutes before the flight batteries require recharging. The longest flight duration completed in this study was approximately 16 minutes (20% battery charge remaining) and covered three plot locations in one flight. This implies slightly better than advertised performance of the system as the sUAS was not hovering in place at any point during the collection. For these collections, a Velodyne VLP-16 lidar was utilized on the sUAS in combination with a differential GPS/INU system for precise tracking. This system integration was designed and completed within the Chester F. Carlson Center for Imaging Science (CIS) at Rochester Institute of Technology (RIT). The sUAS can be viewed, as flown, in Figure 2.2.

The VLP-16 lidar has a pulse rate of 300 KHz and a scan rate of up to 20 Hz. The lidar system has a maximum range of 100 m (~ 328 ft), while the maximum swath width, assuming a -10° to 10° scanning geometry, is 35 m (~ 115 ft). The VLP-16 is capable of 360° scanning, but it is not recommended to use scans at oblique angles for structural mapping [38]–[40]. The VLP-16 is a two return system, recording the first and last return for every pulse, along with reflectance values of targets intercepted by each pulse, also referred to as the intensity value. Point densities achieved were 497.04 - 2,393.93 pts/$m^2$, with a mean point density of 1,504.2 pts/$m^2$. This variance in point density was attributed the flight altitude, changes in flight overlap from plot-to-plot, and degradation in GPS signal, which resulted in a significant number of returns to be removed from the final point cloud. A summary of the lidar system specifications can be found in Table 2.1.


Figure 2.2. MX-1 sUAS remote sensing platform developed by the CIS department at RIT. This configuration included a Velodyne VLP-16 lidar, Mako G-419 RGB camera, and ballast weight in place of the hyper-spectral camera to reduce cost impacts of any mishaps as the hyper-spectral camera was not required for this research.

For the GPS and IMU, an Applanix APX-15 UAV is integrated onto the platform. This is a combined GPS and IMU in a single hardware solution developed specifically for use on sUAS platforms, thereby addressing low mass goals and low elevation tracking requirements. The APX-15 features the capability to employ real-time kinematic (RTK) correction to the GPS positioning data, achieving position error bounds of 2 – 5 cm. This RTK correction is applied to

the IMU data as well, achieving errors of 0.03° for roll and pitch, and 0.18° for yaw. A detailed description of the data collection activities and study sites can be found in the method sections of Chapters 3 and 4.

Table 2.1. Velodyne Lidar Sensor Specifications.

**Velodyne VLP-16**

| | | | |
|---|---|---|---|
| **Laser Altitude** (ft) | 200-300 | **Returns** | ≤ 2 (first and last) |
| **Swath Width** (ft) | 35-52 | **Average Resolvable Horizontal Distance Between Points** (ft) | 1.18 |
| **Scan Rate** (Hz) | 10 | **Footprint** (ft) | 1.57 |
| **Pulse Rate** (KHz) | 300 | **Wavelength** (nm) | 903 |

## 2.6 PRE-PROCESSING METHODS

Prior to processing metrics and models in support of sustainable forest initiatives, a number of pre-processing and conditioning steps of the data are required. In order to generate meaningful structural information, the point cloud elevation values must be normalized to the underlying surface terrain. A few open source tools are available that will ingest lidar data in the ".las" file format and classify ground returns. These ground returns are then used for generation of a digital elevation model (DEM), also known as the digital terrain model (DTM) in some studies. LAStools implements a variation of the ground filtering algorithm based on the triangular-irregular network (TIN) method introduced by *Axxelson*, with low misclassification rates [41], [42]. FUSION/LDV uses a method first introduced by *Kraus and Pfeifer*, based on linear predictions and weighting functions [20], [43]. While this approach has been a suitable method for other studies, the four parameters proved to be difficult to optimize for the data set in this research. The FUSION tool often falsely classified returns from tree stems near the ground as ground, resulting in large spikes within the DEM. The LAStools implementation generated adequate ground classifications for DEM generation, with a single adjustment to the step size of the window used for initial classification.

Once the ground return classification is complete, a DEM can be generated on a raster

grid, using the lowest return in each cell as the elevation. Interpolation is required for grid cells that contain no returns. Common interpolation methods used are Delaunay triangulation with linear interpolation, inverse distance weighting and kriging [44]. LAStools pursues an alternative strategy by generating a TIN from the ground points and then rasterizes the TIN, thus all cells have values within the area enclosed by the ground returns. The high point density nature of the data collected in this study generally did not require any interpolation. If grid cells smaller than 0.5 m were used, then interpolation methods would need to be employed. Once an adequate DEM has been created, all points within the point cloud can be normalized to the DEM. These normalized point clouds, i.e., height-above-ground, are analyzed to generate models and evaluate forest metrics. A depiction of this workflow, from raw to normalized point cloud, can be seen in Figure 2.3.

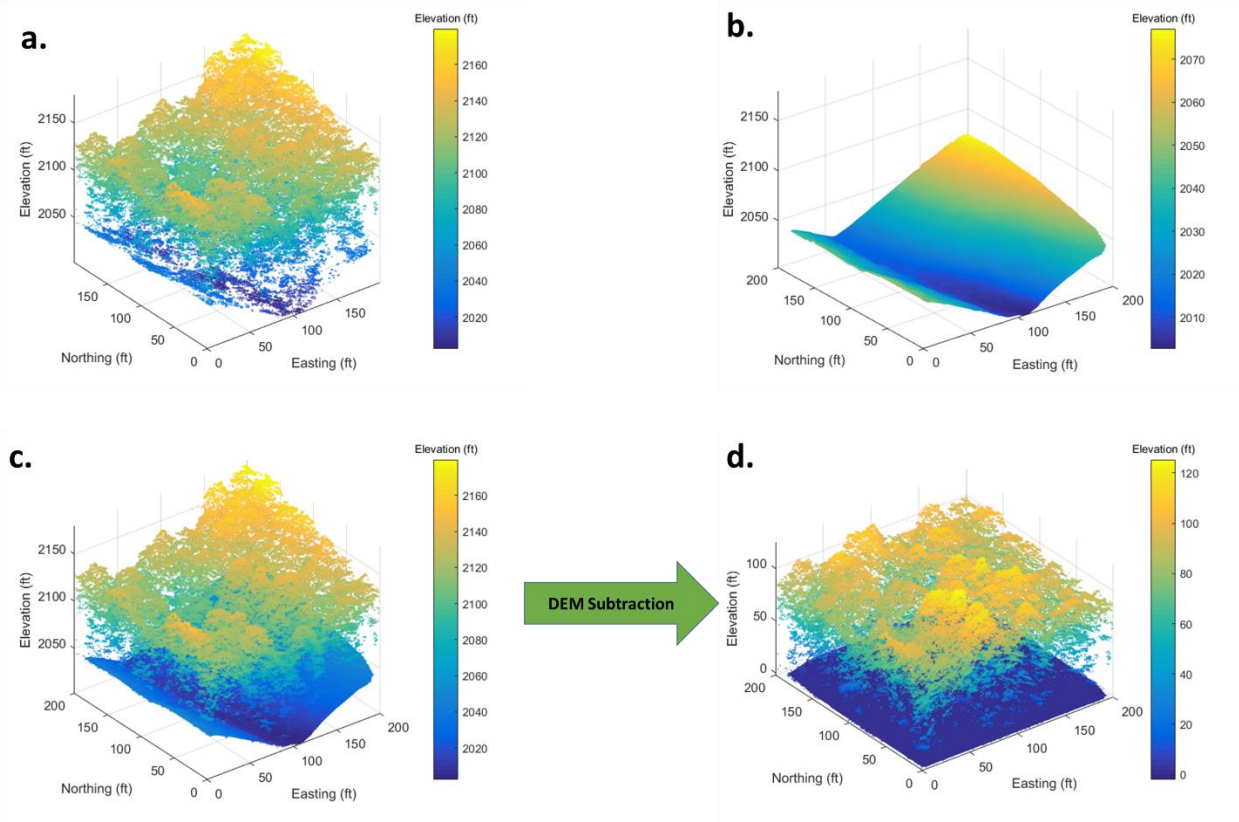


Figure 2.3. Depiction of point cloud normalization processing steps. (a.) Raw point cloud with elevation values referencing mean seal level, (b.) DEM generated from ground-classified points, (c.) Raw point cloud plotted above DEM for visual reference, (d.) Normalized point cloud after DEM subtraction with normalized DEM for visual reference. Elevation values are now expressed as above ground level.

# Chapter 3

# Cost Analysis Between Manned Airborne and sUAS Sensor Platforms

## 3.1 FOREWORD

This chapter represents a paper that was presented and published in the SPIE Commercial + Scientific Sensing and Imaging Conference proceedings, April 2018 [18]. It explores a simple linear regression model for predicting plot level aboveground carbon levels to demonstrate the similar performance of commercial lidar systems and the sUAS systems deployed by RIT. It further analyzed the cost comparison of the two systems. This paper addresses Objectives 1 and 4.

## 3.2 ABSTRACT

Sustainable forest management practices support the growing effort to make efficient use of natural resources without a reduction in future yield potential. These efforts require accurate and timely measurement of the world's forests to monitor volume, biomass, and stored carbon level changes. Historically, these measurements have been effected through manual

measurements of individual trees in representative plots, spaced throughout the forest region. Through the process of imputation, the missing values are interpolated, often through a regression model based on the collected reference data. Remote sensing technologies, specifically lidar (light detection and ranging), possess the capability to rapidly capture structural data of entire forests; however, airborne lidar mounted on manned aircraft can be cost prohibitive. The increasing capabilities and reduction of cost associated with small unmanned aerial systems (sUAS), coupled with the decreasing size and mass of lidar sensors, have opened the possibility for these platforms to provide a cost effective method with comparable performance. This study completes a cost comparison of the two platforms using a regression model of above ground live carbon as a method of comparing performance in context of sustainable forestry. The sUAS performed comparably based on our two data sets. The sUAS achieved a $R^2$ of 0.74, and the manned aircraft lidar system achieved an $R^2$ of 0.61, with both models producing RSE(%) within one percent of each other. The sUAS has the capability to be competitive with the manned aircraft at a cost of $8.12/acre for the study area, compared to the manned aircraft's cost of $8.09/acre. The added benefits of sUAS include rapid deployment and low mobilization costs, while disadvantages include operational considerations, such as the need for line-of-sight operations. However, we concluded that sUAS is a viable alternative to airborne manned sensing platforms for fine-scale, local forest assessments.

## 3.3 INTRODUCTION

In the past few decades, more organizations have embraced the importance of efficient, sustainable usage of natural resources on earth and have taken an active role to embrace sustainable forest management (SFM) policies. The majority of the planet's inhabitants rely on products derived from forestry, along with the ecosystems that these forests support. Recent trends show total forest area loss has been slowing, with the period from 2010 to 2015 showing a forest coverage loss at half the rate as the period of 1990 to 2000 [17]. It has become clear that these resources must be carefully used; otherwise, future generations may not have what is needed to meet the requirements to sustain or increase the current forest product and ecosystem service benefits.

Multiple organizations that have been formed to develop best practices and methods in

regards to sustainable forestry. One example is the UN Framework Convention on Climate Change (UNFCCC), which has the initiative "Reducing Emissions from Deforestation and Degradation" (REDD+). This initiative drives the need for large-area biomass and carbon inventories, and incentivizing the concept of carbon credits [15]. Additionally, 12 host nations that manage 49% of the world's forests, which contain 90% of the world's temperate and boreal forests, follow the Montreal Process for SFM [16]. This process establishes seven criteria as guiding principles, each containing measurable indicators to determine success or failure in maintaining the guidelines as nations. These SFM principles drive a need to accurately capture inventory metrics across large areas and to do so in an expeditious manner [4], as change detection requires repeated measurement.

In the past, these forest measurements have been done exclusively by ground crews, manually measuring each individual tree in representative plots of the entire forest [2]. From these representative plots, the rest of the forest area measurements can be estimated through the process of imputation [3]. Imputation is a process of filling in data points that were not directly measured. This can be done through various methods, with regression modeling being commonly used in the context of forestry [4]. As expected, it can be tedious and time consuming to employ a field crew to measure individual trees in forests covering large areas. It becomes increasingly difficult in rugged, mountainous terrain. Remote sensing technology possesses the capability to execute these measurements in challenging terrain, specifically by using airborne lidar scanner (ALS) systems. A variety of studies at plot and individual tree level have been completed using ALS systems in a variety of forest types and locations, measuring important SFM metrics such as volume, biomass, and stems-per-hectare (SPHA) [11]–[14].

The Rainforest Alliance, an international non-profit organization who describe themselves as "a growing network of farmers, foresters, communities, scientists, governments, environmentalists, and businesses dedicated to conserving biodiversity and ensuring sustainable livelihoods" [45], has developed a partnership with organizations who do business in the southeastern United States (USA) to actively pursue increasing sustainable usage of forests in this region [46]. This section of the USA has a large contingent of small landowners by area, representing a large forested land base, and presenting a unique challenge for gathering required metrics critical to sustainable forestry. Additionally, much of this region is in the Appalachian mountain range and is difficult to access with ground-based vehicles or by foot. Being that these

land holdings are small in size and contain generally difficult-to-navigate terrain, airborne measurements provide the most accessible method for measurement and mapping to support the SFM initiatives.

The current standard for obtaining ALS data for an area of interest is to contract a company specializing in using ALS systems on fixed wing aircraft. Maintaining and operating these systems is an expensive endeavor, and as such, the cost is passed along to the end-users. Studies comparing costs between ground crews manually measuring plot inventory and these airborne scanning systems found that the ALS collections typically cost tens of thousands of US dollars more than a standard ground crew-based collection [2], [3]. The tradeoff, however, is that ALS systems can cover a much larger land area and directly measure entire forests, while the ground crews will measure representative plots and use models to develops estimates for entire forests. Once area is considered, at small area sizes, the ground crew option is more cost effective, but as the area increases the ALS option becomes more competitive [3].

In recent years, reduction in sensor size and mass, coupled with increasing payload capability and flight times of small unmanned aerial systems (sUAS), have provided the opportunity for a third option. This option allows for high operational flexibility at a potentially reduced cost from the typical ALS system deployment. The sUAS is lightweight with a small logistical footprint; there are no recurring fuel costs, and such systems only require a Federal Aviation Administration (FAA) part 107 certified pilot. We hypothesize, that with a sUAS, an organization can obtain the same level of accuracy of the legacy ALS systems and can procure higher density point clouds for use in SFM metric analysis. To test the hypothesis, a data collection was conducted using a commercial ALS system, and a sUAS ALS system, developed by the Chester F. Carlson Center for Imaging Science at Rochester Institute of Technology, both flown in similar and overlapping regions. An above ground live carbon (AGLC) model was developed as a test to compare model performance using both collections, and a cost analysis of the two collections was completed.

## 3.4 METHODS

### 3.4.1 Study Area

Two study areas were flown: The first, of which the majority of the data were collected from, is located on Clinch Mountain in Russell County, VA. This forest covers approximately 4,000 acres and is dominated by steep ridges and narrow valleys. The forests here are of the temperate deciduous type, being mostly composed of eastern USA broadleaf trees. A carbon audit measurement was completed by ground crews in October 2016. The plots measured consisted of 151, 0.1 acre (~0.04 ha), fixed-radius plots, measured in slope-feet, spaced on a regular grid of 1,000 ft (~305 m) apart. In these surveyed plots, 1,949 individual trees were measured. Diameter at breast height (DBH) of vegetation larger than 5" (~12.7 cm) DBH and total height were measured, along with models produced of volume, above ground biomass (AGB), total carbon, and AGLC.

Both the manned ALS system and sUAS were flown in this location. Of the 151 representative plots, 49 plots were covered by the manned ALS system, and 17 by the sUAS. Five plots overlapped, for a total of 54 plots covered. These 54 plots contained 804 individually measured trees. These focus plots were chosen as they contained variability in AGB, harvesting levels, and trees blown over by storms and other natural events. This would allow for a diverse sample set to aid in algorithm development. In these focus plots, vegetation species were predominantly deciduous types. Maple species (*Acer negundo, A. rubrum, A. saccharum*), Yellow Poplar (*Liriodendron tulipifera*), and Oak species (*Quercus alba, Q. coccinea, Q. muehlenbergii, Q. prinus, Q. rubra, Q. stellata, Q. velutina*) dominate the majority of the inventory, comprising 23.63%, 22.76%, 18.66% (65.05% total) of the vegetation present, respectively. This area served as an ideal location to highlight the use of ALS systems for gathering forestry information quickly in difficult to traverse terrain. A map of this location can be seen in Figure 3.1.

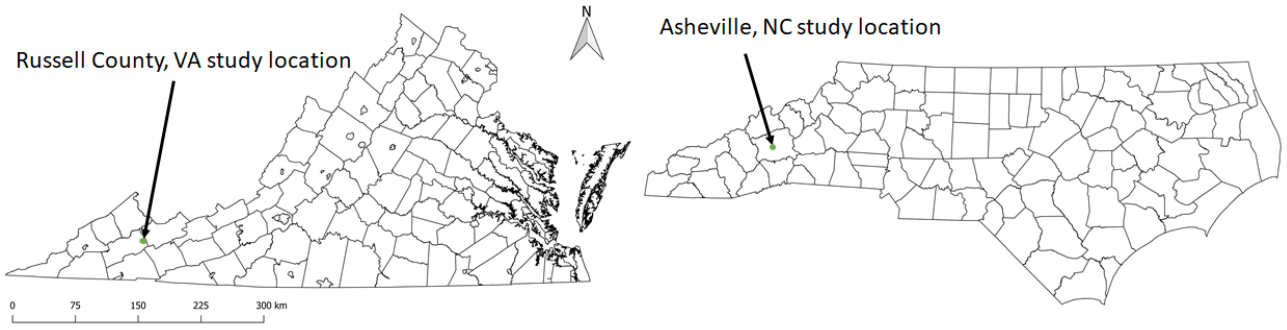


Figure 3.1. Two study areas were used in this project. The first was located in Russell County, VA in the Clinch Mountain Range. Both manned and unmanned ALS systems were flown here. The second study site was located at the Om Sanctuary in Asheville, NC. Only the unmanned ALS system was flown here.

The second location flown was the Om Sanctuary, located in Asheville, NC. A map of this location can be seen in Figure 3.1. This location also proved challenging as it was on the side of a steep slope, where the land area dropped to the river below; it also was dense and difficult to traverse. Similar to the Russell County (VA) location, these forests are of the temperate deciduous type, being mostly composed of eastern USA broadleaf trees. An audit was completed at this location in March 2017. The areas measured consisted of 20, 0.1 acre (~0.04 ha) fixed-radius plots, measuring 345 individual trees. Diameter at breast height (DBH) of vegetation larger than 5" (~12.7 cm) DBH and total height were measured, along with models produced of volume, above ground biomass (AGB), total carbon, and AGLC. Only nine plots had tree height values reported, all other measures and models were produced for all 20 plots. These nine plots contained 149 individual samples.

Only the sUAS was flown at the Asheville location due to budget constraints. Of the 20 representative plots, nine were covered by the sUAS, as these were the only plots with height reference data. This location presented a more diverse species mixture among the focus plots: Yellow Poplar (*Liriodendron tulipifera*), Sourwood (*Oxydendrum arboreum*), Chestnut Oak (*Q. prinus*) and Red Maple (*A. rubrum*) were the three largest contributors, comprising 26.17%, 15.44%, 11.41%, 11.41% (64.43% total) of the vegetation present, respectively. A notable difference of these plots is the presence of conifers. Two species (*Pinus strobus* and *P. rigidia*) were present, totaling 11.41% of the vegetation. This area served as an adequate supplement to continue development of the sUAS models.

### 3.4.2 Data Collection

The manned ASL data collection was completed on 20 July, 2017 over the Russell County, VA site. For the manned ALS system, the work was completed by a commercial vendor who flew a Leica ALS80 discrete return lidar on a fixed wing aircraft at approximately 7,850 ft (~2,400 m) AMSL. This sensor has a pulse rate of 1 MHz and a scanning rate of up to 200 Hz and is capable of recording 8 km swaths from high altitude flights. This flight was a mid-altitude flight, as we had requested a higher density point cloud with flight path overlap. The point clouds we received were five return-per-pulse, with the first three returns inclusive of associated intensity values. Point densities over the focus plots achieved using this configuration were in the range of 30.44-99.16 pts/$m^2$, with an average point density of 71.19 pts/$m^2$. The inconsistency between point density can be traced back to an inconsistent flight overlap in the vicinity of the actual plot locations.

The sUAS ALS data collections were completed on 11 and 13 August 2017 at the Russell County, VA location and on 12 August 2017 at the Asheville, NC location. An example point cloud generated from this collection with the maximum point density can be seen in Figure 3.2. The platform used for the sUAS was a DJI Matrice M-600 Pro, with a custom payload rig capable of lifting a modular sensor platform. This setup is capable of flying for approximately 18 minutes. The longest flight completed in this study was approximately 16 minutes and covered three plot locations. For these collects, a Velodyne VLP-16 lidar was utilized on the sUAS in combination with a differential GPS/INU system for precise tracking. This system integration was designed and completed in the Chester F. Carlson Center for Imaging Science at Rochester Institute of Technology. The flight altitude varied from 200 – 300 ft (~60-90 m) AGL, since the flight software for flight planning was not precise while in terrain following mode. In-flight variation was less than 10 ft (~3.3 m), but the manner by which the flight software set the target height was variable at each location. The VLP-16 lidar

Figure 3.2. Example point cloud at 2,000+ pts/m2. This point cloud was generated with RIT's sUAS remote sensing platform.

has a pulse rate of 300 KHz and a scan rate of up to 20 Hz. The lidar system has a maximum range of 328 ft (100 m), the maximum swath width, assuming using -10° to 10° sight lines like that of the ALS80, is 113 ft (~35 m). The VLP-16 is capable of 360° scanning, but it is not recommended to use scans at oblique angles for structural mapping, as it introduces error and occlusions [38]–[40]. The VLP-16 is a two return system, recording the first and last return for every pulse, along with associated intensities. With this system, point densities achieved were 497.04-2,393.93 pts/m2 with a mean point density of 1,504.2 pts/m2. This variance in point density was attributed the flight altitude, changes in flight overlap from plot to plot, and degradation to GPS signal, which resulted in a significant number of returns to be removed from the final point cloud. A summary of both lidar system specifications can be found in Table 3.1.

Table 3.1. Lidar sensor specifications as flown.

| | **Leica ALS80** | **Velodyne VLP-16** |
|---|---|---|
| **Laser Altitude** (ft) | 7,850 | 200-300 |
| **Swath Width** (ft) | 1,800 | 35-52 |
| **Scan Rate** (Hz) | 120 | 10 |
| **Pulse Rate** (KHz) | 1000 | 300 |
| **Returns** | ≤ 5 | ≤ 2 (first and last) |
| **Average Resolvable Distance Between Points** (ft) | 4.72 | 1.18 |
| **Footprint** (ft) | 4.02 | 1.57 |
| **Wavelength** (nm) | 1064 | 903 |

### 3.4.3 Cost Analysis

The main hypothesis of this paper was that sUAS ALS systems provide a cost-effective alternative to current manned aircraft systems, without sacrificing model accuracy and generating higher density point clouds. It has already been shown that the sUAS is capable of generating higher density point clouds. This section will outline how we approached the cost analysis. Two studies were referenced for cost comparison; however, one was more recent and provided a thorough cost breakdown of tasks associated with gathering timber measurements [2],

[3]. The main logic for determining cost was modeled after the study that Hummel et al. completed when comparing ground measurements costs to that of ALS systems at the time [3]. Their study included a breakdown of cost by work hour, using the US Federal General Schedule wage tables as a stable pay standard for task-by-task costs. This methodology was continued, utilizing the 2018 General Schedule [47], and adjusted to match the tasks required in this study. Table 3.2 shows the breakdown of additional cost that is in addition to procuring the fly over by the manned flight.

Table 3.2. Planning and processing cost breakdown for each ALS system.

| Processing task | No. of days manned aircraft | No. of hours manned aircraft | No. of days sUAS | No. of hours sUAS | Worker grade level | Average rate ($/hr) | Average cost manned aircraft ($) | Average cost sUAS ($) |
|---|---|---|---|---|---|---|---|---|
| Project Management | 20 | 160 | 10 | 80 | 12 | 34.54 | 5526.40 | 2763.20 |
| Data Preprocessing | 3 | 24 | 2 | 16 | 9 | 23.82 | 571.68 | 381.12 |
| Remote Sensing Data | 1 | Fixed Price | 3 | 48 | 9 | 23.82 | 7200.00 | 1143.36 |
| Geospatial Join | 2 | 16 | 2 | 16 | 9 | 23.82 | 381.12 | 381.12 |
| Feature Space | 5 | 40 | 5 | 40 | 12 | 34.54 | 1381.60 | 1381.60 |
| Modeling | 5 | 40 | 5 | 40 | 12 | 34.54 | 1381.60 | 1381.60 |
| Validation | 3 | 24 | 3 | 24 | 12 | 34.54 | 828.96 | 828.96 |
| Product Deliverables | 10 | 80 | 10 | 80 | 9 | 23.82 | 1905.60 | 1905.60 |
| Total | | 224 | | 264 | | | 19176.96 | 10166.56 |

There are major differences from what Hummel et al. completed in their analysis [3]. They encompassed the ground collection cost and the processing of the lidar data. Our analysis simply covers the cost of procuring the lidar from both systems and processing it. The ideal concept of operations would be to cover all plots with both systems, thus rendering the effect of the cost of procuring reference data to be null. In our study, however, the data were utilized without cost to the user. If one wishes to add the ground reference procurement, Hummel *et al.*

provide a general cost/acre that could be used, and an adjustment for inflation would be required [3].

### 3.4.4 Modeling Methods

Both lidar data sets were delivered in an unclassified point format, and in differing coordinate systems, neither of which were in the coordinate system of the supplied plot locations for the ground reference plots. This required that each data set be processed through a ground classification algorithm. This is necessary so that each lidar return could be normalized to height above ground. Both of these steps were completed using the software suite LAStools [42]. The ground classification was completed using the function *lasground_new* with a step size selection of nine meters, and the coordinate transformations were completed using the function *las2las*.

Buffers matching the fixed plot radius (37.5 ft; ~11.4 m), as used in ground reference data collections, and square buffers measuring 115 m x 115 m were developed in the QGIS software suite [48], prior to clipping the full point clouds to the specific plot locations,. The square buffers were used to reduce the point clouds to manageable sizes for ground classification and normalization using LAStools, as most files contained >10 million points. Such large buffers avoid interpolation edge artifacts on the digital elevation model (DEM) produced. The clipping of the point clouds was completed using *polyclipdata* from the FUSION software suite [20]. This software allows for lidar file clipping using a shapefile that contains multiple polygons, and outputs individual lidar point cloud files for each plot location.

A regression analysis was run on the final point clouds, similar to that used by Means *et al.*, with the major difference that this regression was applied to the point clouds themselves, rather than rasterized grids of the point clouds [2]. Statistical (distribution) values of each point cloud was calculated, such as maximum height, mean height, minimum height, kurtosis, skewness, and percentiles, ranging from the 5th to 95th percentiles in 5 percent increments. The same treatment was applied to the intensity values. In order to be included in the final models, the predictor variables were required to have an F statistic with significance level of 0.05 or less. Variables were removed in subsequent steps if their significance level rose above 0.1. Even though the removal criteria were larger than the entrance criteria, no model run resulted in a predictor variable with a significance above 0.05.

A challenge for this study was that the two data sets cover similar, but not identical areas.

A review by Zolkos et al. of 70 publications on AGB models found that expressing the Residual Standard Error (RSE) of a model in terms of the mean AGB (RSE(%) = RSE/μAGB) value, constitutes a satisfactory means of comparing studies in different regions [49]. The authors furthermore noted that studies in temperate deciduous forests had an average RSE(%) of 31% [49]. Finally, in the Means et al. study, it was found that heteroscedasticity existed in their models of basal area and volume [2]. Their solution was to model the natural logarithm of these dependent variables, resulting in improved performance. A similar condition was noted with the AGLC models in this study, thus an alternate model of the natural logarithm of the measurement data was implemented as well. Similar improvements to the error values was seen, but not in the $R^2$ values.

## 3.5 RESULTS AND DISCUSSION

### 3.5.1 Above Ground Carbon

Results of the models derived from the two data sets can be seen in Figure 3.3, and the predictive equations produced can be seen in

Table 3.3. While the sUAS appears to outperform the manned aircraft approach, such an observation should be cautiously evaluated. This is due to the data sets not containing the exact same reference data from their different flight area extents. There is an overlap of five similar plots, which is a minority for each data set. This discrepancy is a result of extremely difficult terrain to launch the sUAS in and the FAA requirement of maintaining a line-of-sight (LOS) on the sUAS during flight, which can be difficult in mountainous forests. We noted that increases in power supply, to allow for longer duration flights from the established landing zones, would enable more plot coverage by the sUAS.

However, the two data sets do cover similar forest types, so it is valid to state that they performed similarly in this study. It was concluded, based on the RSE(%) metric, that both platform types had comparable performance, as in both model forms the two data sets produced an error within one percent of each other. For both scenarios, manned vs sUAS lidar platforms, modeling the natural logarithm of the reference data resulted in a marginally better fit (increased $R^2$ values). The RSE(%) is misleading in the logarithmic space due to the reduced magnitude of the values being modeled, the important take away is that they are similar across platforms.

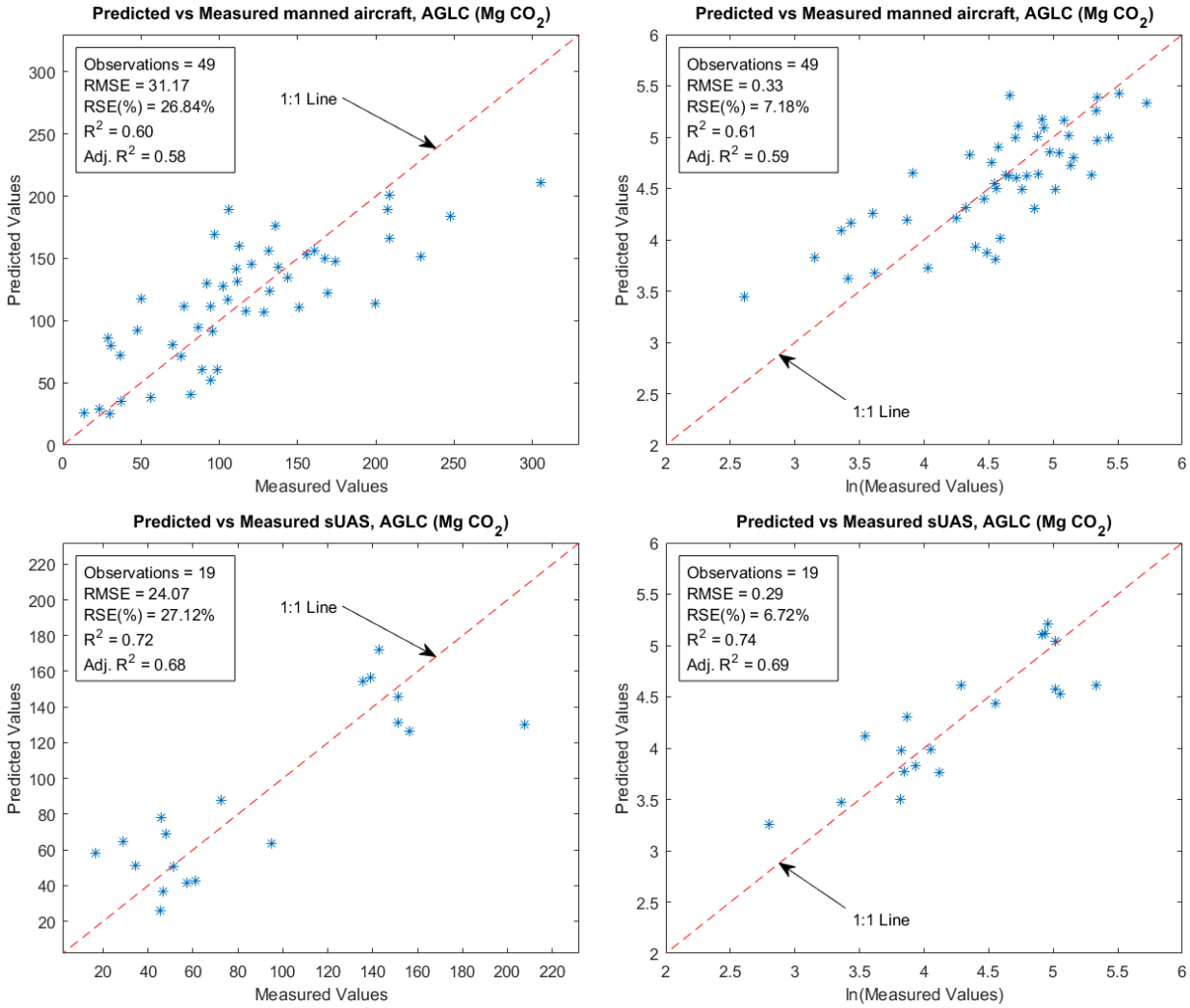


Figure 3.3. Predicted vs measured plots, depicting the performance of the linear regression models developed from the two available data sets. The top row shows results from the manned aircraft data collections and the bottom row contains the results from the sUAS data collection. The left column depicts the models based on the raw measured AGLC values, while the right column depicts the models derived from the natural logarithm of the measured AGLC values.

Table 3.3. Regression models of AGLC and ln(AGLC) using the two data sets. MedHt is the median height. Ht25ile is the 25th percentile of the height. MaxInt is the maximum intensity. Int5ile, Int55ile, and Int70ile are the 5th, 55th and 70th percentile of the intensity. All of these measures come directly from the point cloud.

| **Sensor Platform** | **Regression Equation** | **$R^2$** | **RSE(%)** |
|---|---|---|---|
| Manned Aircraft | AGLC = -156.4 + 5.989*MedHt + 0.0035*MaxInt - 0.027*Int5ile | 0.6 | 26.48 |
| Manned Aircraft | ln(AGLC) = 3.58 + 0.0638*MedHt - 0.000236*Int5il | 0.61 | 7.18 |
| sUAS | AGLC = -112.15 + 4.87*Ht25ile + 0.0087*Int70ile | 0.72 | 27.12 |
| sUAS | ln(AGLC) = -0.93+ 0.19 Ht25ile + 0.000317*Int55il + -9.28E-6*Ht25ile*Int55ile | 0.74 | 6.72 |

### 3.5.2 Costs

The cost analysis continued to be a valid interest, given that both data sets produced valid results for modeling a timber metric important to SFM. A breakdown of collection activity planning and data processing costs can be seen in Table 3.2. A major discrepancy between the two types of collection is that there is more program management involved with establishing a contract with a commercial vendor and coordinating data sharing, when compared to a solution within the organization. At a minimum, a two-person team typically deploys to complete the collection with the sUAS, so the hourly rate for this task is effectively doubled. The cost of procuring the manned aircraft lidar collection was $7,200, this does not include the typical mobilization cost as it was completed on an already scheduled flight. The final cost of the manned system was ~$19,180, while the sUAS lidar does encompass all of the processing and procurement of data, thus the total cost is ~$10,167.

At first glance, the sUAS is cheaper in total cost; however, the sUAS only covered 19 plots. The average cost per plot was then ~$535, which would imply a final cost of ~$26,219 for the total 49 plots. This is significantly more expensive than the manned aircraft collection. To gain insight as to why this is, we can break down the cost by area covered, as done by Hummel *et al.* [3]; *we will report results in US$/acre, for clarity sake*. In their study they found that they achieved an average cost of $3.03/acre, and adjusting for inflation that translates to $3.60 in 2018 dollars [50]. The manned aircraft lidar covers an area of 2,372 acres, for a cost per acre of $8.09. The sUAS lidar covers an area of 417 acres, which leads to a cost per acre of $24.36, just over three times as expensive as the manned aircraft collection. Both of these rates are higher than what was found in the referenced study, but the coverage area for our study was less than half of theirs, and the cost per acre increases as your study area decreases, since the overhead associated with collecting does not change significantly.

This insight may lead to one drawing the conclusion that the sUAS currently cannot compete with the legacy methods. However, a small detail should be considered in this cost analysis. For this particular collection, a study for structure-from-motion was being conducted on the same flights. This reduced the maximum flight speed to avoid motion blur in the imagery, requiring a flight speed three times slower than that required to match the point density generated

by the manned aircraft. With a fixed flight time, due to battery life on the sUAS, this limited the number of plots and in turn the area that can be covered per flight. Not only did this reduce the coverage area, it also increased the number of hours the flight crew had to work to cover the study area, further driving up cost. Factoring this in and tripling the area that the sUAS can cover, i.e., up to 1251 acres, the per acre cost drops to $8.12, which is competitive with the manned aircraft system. It is noted that manned aircraft costs do not linearly drop with coverage reduction, since much of the cost is associated with the system itself and not with the flying time. At small acreage levels, as is the case with the small landowners in southeastern USA, the sUAS thus is a viable option.

## 3.6 CONCLUSIONS

The need for efficient and sustainable societal use of natural resources available has become more pronounced in recent times. Sustainable forest management (SFM) policies standardize forest resource usage in such a manner that theoretically will result in perpetual growth and yield potentials. In recent years, a positive change has been observed due to these policies, with deforestation rates dropping, although much work has yet to be done to ensure that such approaches become common practice [17], e.g., via SFM initiatives such as REDD+ or the Montreal Process [15], [16]. However, we need accurate and precise approaches to forest inventory and mapping.

Forest timber measurements in the past have been completed by ground crews who manually measure each individual tree in representative plots of the entire forest [2], after which the forest inventory for the rest of the forest area is modeled (estimated), based on such sampled plots [3]. This is commonly done through volume of biomass regression models [4]. However, it can be tedious and near impossible to complete the measurements on the ground in rugged, mountainous terrain. Remote sensing technology, such as ALS systems, therefore presents an opportunity to more efficiently measure forests and access areas that cannot be reached by conventional methods. Many studies have been evaluated the assessment of timber metrics, such as volume, biomass, and stems-per-hectare using ALS systems [11]–[14]. The southeastern US is an especially ideal candidate area for employing this technology, since this region has high volumes of manageable timber, and consists many small land owners scattered amongst difficult

terrain in the Appalachian Mountains.

Currently, it is standard practice to contract a company to fly an ALS system, mounted on a manned fixed wing aircraft, to generate lidar data of the interest areas. These systems are expensive to field and maintain, with studies showing that they are not economically advantageous to deploy for small land coverage/areas [3]. However, ALS systems are capable of covering the entire interest area and not just the measured reference plots, providing an opportunity to directly model the entire forest. It is in this context that sUAS systems are poised to compete with the manned aircraft option, since flight times and payload handling capabilities have increased in the past few years, while sensor mass, volume, and cost have been decreasing. We therefore contrasted an airborne vs. sUAS ALS approach for forest carbon modeling.

To validate our comparison, both types of systems were flown over areas with AGLC data available. Two sites were used, one in Russell County, VA and another in Asheville, NC. 49 plots were covered by the manned system and 19 plots were covered by the sUAS. There was an overlap of five plots between the two data sets. A linear regression of the AGLC and natural logarithm of the AGLC were completed, based on independent variables extracted from lidar return distributions for the resulting point clouds. The sUAS approached produced a larger $R^2$ value of 0.74 vs. the 0.61 produced by the manned aircraft data set. This was not considered to be a definitive result, however, since the sample sets did not cover the same area. The RSE(%) therefore was used for comparison, as defined by Zolkos *et al.* [49]. In reference to RSE(%), the models from each data set were within one percent of each other, i.e., we concluded that they performed similarly.

With regards to absolute cost, the sUAS was the more cost-effective option at $10,166.56 vs. the $19,179.96 for the manned ALS system. This was largely due to covering a smaller area, namely 417 acres vs. 2,372 acres. Once cost per acre is considered, the relationship was reversed. The manned aircraft came in at $8.09/acre, while the sUAS was just over three times that, i.e., $24.36/acre. It was noted, however, that the sUAS collection was at a reduced flight speed to account for a 3D, structure-from-motion imagery project on the same flight. If the flight speed were optimized for a lidar-only data collection, the cost then would have been $8.12/acre for the sUAS. This would result in lower density point clouds, but they would still exceed the point density of the manned aircraft system. In reference to our hypothesis, we have shown that the

sUAS data i) were of higher density and ii) produced comparable models. However, we did not conclude that it was more cost effective; at best, sUAS was deemed as roughly the same cost as the manned ALS system.

Improvements that could be made to reduce the cost of sUAS deployments would be to increase flight time capabilities, in other words, higher capacity power sources. The 18-minute battery limit reduced the flight time and increased the amount of time that the aircraft needed to be serviced by the ground crew. Additionally, the LOS requirement proved to be a major hindrance during the collection operations. If organizations wish to utilize sUAS ALS systems regularly, they should consider permanent or mobile observation structures for maintaining better sight lines. The pilot is not required to maintain sight of the vehicle, only the safety spotter, and the majority of sUAS employ an onboard camera for maintaining situational awareness. sUAS ALS forest applications have significant potential, and we expect the cost to continue to decrease for these systems, thereby allowing for easier procurement and fielding of systems.

# Chapter 4

# Carbon Modeling and Plot Disturbance Detection

## 4.1 FOREWORD

This chapter introduces a functional carbon model based on canopy height distributions, derived from lidar canopy height models. A comparison is completed between a commercial lidar system and sUAS lidar system, with an additional comparison between lidar and structure-from-motion (SfM) methods from each platform. Additionally, a classifier is developed to detect disturbed plots and flag potential harvesting. This chapter is written with the intent to publish in a journal within the 2018 – 2019 timeframe and addresses Objectives 1, 2 and 3.

## 4.2 ABSTRACT

Sustainable forest management relies on the acquisition of timely (change detection) and accurate structural information of the forest landscape. Light detection and ranging (lidar) remote sensing platforms provide the capability of rapid 3D, structural data collection with high spatial resolution. In this study, we explore a functional biomass model that was initially developed on

synthetic reference data, and here for application in a dense, closed deciduous forest in the southeastern United States. Data were collected by both manned airborne and sUAS lidar systems, with the manned system producing a more comprehensive data set due to a larger coverage area. Both systems produced high-density lidar point clouds, with the manned system exceeding 30 pts/$m^2$ and the sUAS exceeding 400 pts/$m^2$. A hybrid approach of combining cost-effective structure-from-motion generated point clouds with lidar-derived DEMs was also explored. The functional carbon model uses a dot product of the canopy height distribution, defined as the percentage of ground covered by vegetation at various heights, and a trained weighting function to predict biomass, or carbon at the plot level. For our study, results were comparable to those achieved by the initial developers ($r^2$ = .64 vs $r^2$ = 0.72), even given the deciduous species of our study sites. Their application, in contrast, was on a coniferous forest plantation with a more homogenous canopy than what is found in this study's natural heterogeneous forest. With this in mind, our application showed potential for expanded use and performed better than the standard linear regression models applied previously to this data set. Additionally, through examining vertical profiles mapped by generating per-grid cell point density through a voxel method, a binary classifier was trained to successfully detect potentially harvested sites. The Producer's accuracy, User's accuracy, and Kappa statistic for this disturbed plot detection were 94.1%, 92.2% and 89.8%, respectively, showing a high likelihood of detecting disturbed (harvested) plots. These results should be used with caution, however, as there were only seven examples of harvested sites to train and test on. A robust leave-one-out and holdout cross validation methods were used to train and test the classifier, using 1000 trials, with the results presented in this study being the mean values over all trials. The results demonstrated that this method has the potential to be a valuable tool for organizations interfacing with small landowners, such as those found in the southeastern United States, and for assessing compliance with sustainable for management principles.

## 4.3 INTRODUCTION

Forests traditionally have supplied resources used by the majority of civilizations, while also storing carbon, sheltering wildlife, and aiding in climate regulation [51], [52]. Managing these forests in a sustainable manner require timely and accurate measurement methods, for change detection and quantification needs, respectively [27]. It is in this context that remote

sensing utilizing laser scanning systems, known as lidar (light detection and ranging), have come to the fore. Lidar systems have reached a maturity level to where they may be considered a standard data source for structural measurements of forests [28], [53], [54], where the forest structural elements refer to the spatial arrangement in three dimensional space, the distribution of, and abundance of vegetation in a scene [55]. Lidar systems generate three-dimensional point clouds, depicting scene structure by emitting a laser pulse and measuring the time delay of the return pulse to directly measure a distance from the sensor [19]. If the initial pulse location and direction of the pulse is known, a three dimensional point cloud of measurements can be generated to describe the scene that is being assessed.

Initial remote sensing approaches to forest measurements focused on passive electro optical sensing or synthetic aperture radar, but both methods struggled to produce adequate results (accurate and precise) for older or heterogeneous forests [5]–[8]. The utility of lidar in this domain has be demonstrated going back over 50 years [21]. The structural measurements made by lidar systems can be used for measurement of many forest characteristics, including biodiversity information, stems per hectare, canopy statistics, biomass estimates, and carbon estimates [11], [12], [14], [22], [23]. The multi-return nature of the lidar system allows for the capture of structural information of heterogeneous and older forest growth that the early methods failed to characterize. Furthermore, these types of 3D structural measurements support the sustainable forest principles identified by the Montreal Process and REDD+ initiatives [16]. Both methods drive a need for temporally recurring measurements of forests to monitor carbon, biomass, and biodiversity changes [15].

A well-known hindrance to using airborne laser scanning (ALS) versus a traditional ground crew, direct measurement method, is cost [24], [25]. ALS collections on fixed wing aircraft typically cost tens of thousands of US dollars more than a standard ground crew-based collection for a typical forest extent [2], [3]. A growing alternative to the commercial fixed wing aircraft approach is the small unmanned aerial system (sUAS), which is defined by the Federal Aviation Association as an unmanned aircraft weighing less than 55 lbs at time of takeoff [26]. In recent years, there has an be an increase in the use of sUAS platforms for remote sensing of forests, with *Jaakkola et al.* producing one of the earliest sUAS ALS systems for forest management in 2010 [18], [24], [25], [27]–[29], [56]. This increase in use can be attributed to a few advancements: the increased payload and flight time capability seen with the modern sUAS,

a reduction in sensor mass of cameras, lidar systems, and GPS/INU (inertial navigation unit), and an increase in GPS/INU accuracy in placement of the airframe and characterization of the airframe's attitude during flight (roll, pitch, and yaw). All of these factors allow for larger areas to be imaged, while enabling high quality data products to be generated from these platforms with an ability to fly daily at a low cost of operation [18].

In the earliest example, the flexibility of utilizing a sUAS allowed for the generation of high-density point clouds(100-1500 pts/$m^2$), leading to accurate structural measurement not typically seen with lower density measurements (height bias = -1.6 cm) [24]. These data were then used to validate the application of sUAS data for biomass change and defoliation, resulting in a fit of $r^2$ = 0.92, and demonstrating the utility of sUAS lidar system for forest metric generation and analysis. Early examples of sUAS lidar systems, generating relatively low point densities of 8 pts/$m^2$, demonstrated adequate accuracy levels in tree location with an uncertainty of 53 cm, which is on the order of ground crew accuracies [25]. This high density measurement capability, and the flexibility of flight duration/scheduling that the sUAS provides, lends itself to application within change detection, demonstrating an ability to achieve point accuracies within specified requirements of governmental surveying and mapping standards [40], [57]. *Wallace et al.* found that with only 50 pts/$m^2$, compared to the higher density values of 100-1500 pts/$m^2$, the sUAS platform is able to reliable repeat forestry measurements over 10 flights of the same scene (mean height error of individual crowns = 35 cm), noting the applicability of the sUAS data product to be used for plot level studies, as well as tree-level measurement [28]. This tree-level measurement capability is highlighted in a later study, which achieved a 98% detection rate of individual crowns by utilizing a high density point cloud generated from the same sUAS lidar system [27]. With this level of capability to measure fine structural detail, at the tree- and plot-level, we expect the sUAS system to perform well in this plot-level study.

There are two common approaches to generating three dimensional point cloud products with a sUAS. The first and lower cost solution is structure-from-motion (SfM). This method has been more prevalent in sUAS studies due to the reduced cost to procure adequate cameras and recent increase in computing power, which enabled the processing of large image quantities required for typical forest extents [35], [56]. SfM products can be derived using a common RGB camera, by acquiring overlapping imagery from multiple viewpoints. Modern software packages have been developed, using computer vision algorithms, to detect matching points in overlapping

images and then use standard photogrammetric methods for height extraction of each stereo/overlapping point [34], [35]. sUAS systems are well suited to SfM missions, especially rotor type sUAS air frames, as they are capable of capturing hundreds to thousands of images of the target scene with large overlap, 360° coverage, and minimal motion blur. A disadvantage of the SfM methods is that in order to gather a height measurement of a target, it must be in the unobstructed view of the camera from multiple perspectives. A dense, closed canopy forest presents a significant challenge to this type of measurement, since it typically is difficult to detect enough ground points for height normalization, resulting in a need for an externally-sourced digital elevation model (DEM) [24], [25], [34], [36], [37]. The second method for forest structural characterization is to use a lidar system mounted on the sUAS. This method has the advantage of measuring multiple returns, which enables the analyst to gather much more information about the underlying canopy and terrain. Generally, the terrain models generated from ALS are more accurate than those generated from SfM methods [36].

The typical method of generating models for estimation of plot-level forest metrics is to use a form of regression analysis on a group of selected statistics, generated from the lidar/SfM point clouds themselves or digital surface models, often referred to as canopy height models (CHM), to predict ground measured values for the imaged plots [58]. Once these models have been validated, they can be applied to entire forests, assuming the whole forest has been imaged [59]. This type of analysis has been proven and generally performs well on the study sites that the models are developed on [60]–[62]; however, many models lack common predictors and they do not perform well when applied to other types of forests [58]. *Zhao et al.* proposed a functional model that derived biomass predictions from canopy height distributions, in turn extracted from the CHM of each study plot. This approach showed an ability to maintain performance across scale changes and over a temporal period of four years [58], [63]. The first examples were trained and tested on synthetic field data, aggregated from individual tree estimations [58]. During this study, it was found that the model performed well ($r^2$ = .823 - .938, RMSE = 14.6 – 33.7 Mg/ha) across varying plot sizes (0.01 – 1 ha). A more recent follow-up study explored the application of this model to real reference data, while simultaneously investigating the temporal utility of the model for biomass predictions at future dates in the same region [63]. The training and testing data were sourced from a coniferous plantation in Scotland, comprised of smooth terrain and dominated by Sitka spruce (*Picea sitchensis*), with additional contributions from

European larch (*Larix decidua*), Norway spruce (*Picea abies*), and Lodgepole pine (*Pinus contorta*). In this context, the model performed well in predicting initial data ($r^2 = 0.72, RMSE = 21.5$ Mg/ha), and predicting biomass at later dates for the same region ($r^2 = 0.90, RMSE = 15.7$ Mg/ha). The ability to train the model on one set of dates from a previous data collection and predict biomass on the same region at a later date has direct applicability to the carbon monitoring portion of sustainable forest management principles.

The primary objectives of this paper are to i) implement a comparison of carbon models derived from sUAS vs. manned airborne lidar/RGB cameras for a dense, heterogeneous deciduous forest located in the southeastern United States (USA) and ii) assess the efficacy of a structural detection algorithm, based on sUAS vs. manned airborne systems, to differentiate between disturbed (harvested) an intact forest plots, all toward mapping potentially harvested sites as a means to ensure compliance with sustainable forest management principles. Both ALS and SfM data products were produced for both platforms. The comparison was done by using a functional model, described by *Zhao et al.*, to generate a carbon model of each plot measured by both platforms [58], [63]. In support of the second objective, a detector is implemented as a binary classifier using descriptions of the vertical distributions of each plot from voxels obtained by the ALS systems. The detection of harvested sites is of use to larger forest product organizations who interface with smaller landowners, which are abundant in the southeastern USA, to monitor compliance with sustainable forest management principles.

## 4.4 METHODS

### 4.4.1 Study Area

This study covered two different locations. The majority (84%) of the data collected were on Clinch Mountain in Russell County, Virginia, USA. The Clinch Mountain study area covers approximately 4,000 acres (~1,646 ha) and is rugged terrain comprised of steep ridges and narrow valleys. Temperate deciduous species dominate the forests here, comprised mostly of eastern USA broadleaf species. Reference data were collected in the form of a carbon audit by ground surveyors in October 2016. The audit measured 151, 0.1 acre (~0.04 ha), fixed-radius plots, measured in slope-feet, spaced on a regular grid of 1,000 ft (~305 m) apart across the mountain's face, and inventorying a total of 1,949 individual stems. Diameter at breast height

(DBH) of vegetation larger than 5" (~12.7 cm) and total height were measured, along with models produced of volume, above ground biomass (AGB), total carbon, and above ground live carbon (AGLC).

Both the manned and sUAS ALS systems were flown in this location. Of the 151 representative plots, 49 plots were covered by the manned ALS system and 17 by the sUAS. Five plots overlapped between the two sensor platforms, for a total of 54 plots covered. These 54 plots contained 804 individually measured trees. These focus plots were chosen, since they contained variability in AGB, harvesting levels, and trees blown over by storms and other natural events. This would allow for a diverse sample set to aid in algorithm development. The vegetation species in these focus plots were predominantly deciduous types, comprised mostly of the following species: Maple species (*Acer negundo, A. rubrum, A. saccharum*), Yellow Poplar (*Liriodendron tulipifera*), and Oak species (*Quercus alba, Q. coccinea, Q. muehlenbergii, Q. prinus, Q. rubra, Q. stellata, Q. velutina*) comprising 23.63%, 22.76%, 18.66% (65.05% total) of the vegetation present, respectively. There were only three (0.37%) examples of Eastern Red Cedar (*Juniperus virginiana)*, the lone coniferous species, at this study site. This area served as an ideal location to highlight the use of ALS systems for gathering forestry information rapidly in difficult-to-traverse terrain. A map of this location can be seen in Figure 4.1.

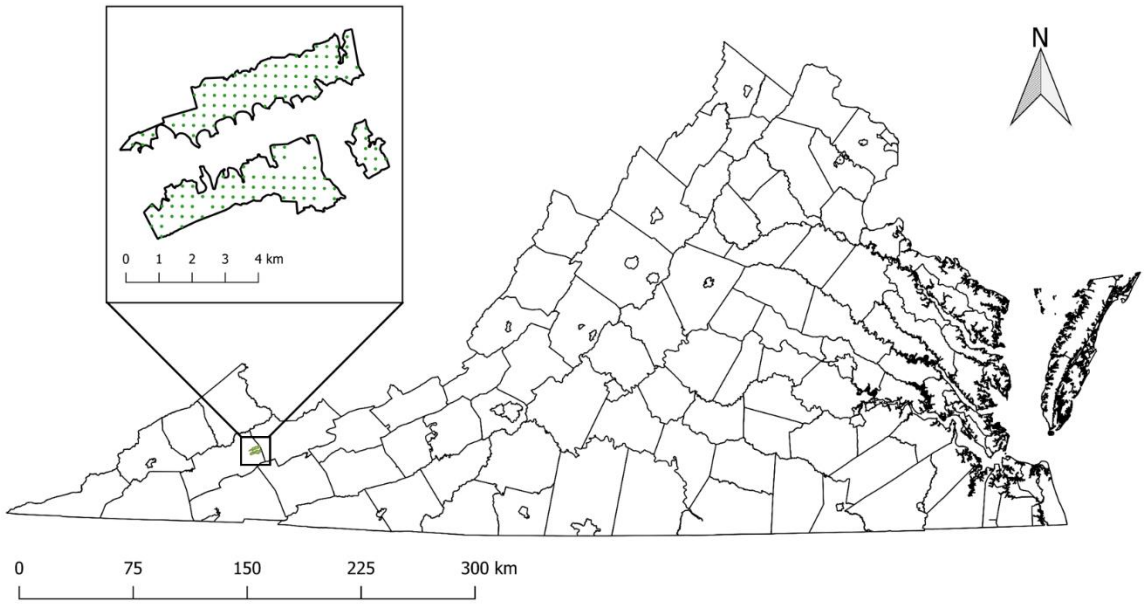


Figure 4.1. Clinch Mountain study site located near Lebanon, VA. The green points are the locations of the measured inventory plots. The majority of data used in this study came from this conservation site.

The second study area was the Om Sanctuary, in Asheville, North Carolina, USA. A map of this location can be seen in Figure 4.2. This site was much smaller than the Clinch Mountain study area, covering only 42 acres (~17.2 ha). Only the sUAS was flown at the Asheville location due to budget constraints, thereby highlighting an advantage to having access to a capable sUAS platform. Nine of the 20 available plots were imaged by the sUAS, as these nine were the only plots with adequate reference data compiled. This location was comprised of a more diverse species mixture among the focus plots with the largest contributors being: Yellow Poplar (*L. tulipifera*), Sourwood (*Oxydendrum arboreum*), Chestnut Oak (*Q. prinus*) and Red Maple (*A. rubrum*) comprising 26.17%, 15.44%, 11.41%, 11.41% (64.43% total) of the vegetation present, respectively. A notable difference of these plots from the Clinch Mountain site is the presence of conifers. Two species (*Pinus strobus* and *P. rigidia*) were present, totaling 11.41% of the vegetation. This is much larger than the 0.37% coniferous contribution at the other study site. This area served as a supplement to continue development of the sUAS models after data corruption reduced the sample size of imaged plots in the Clinch Mountain location.

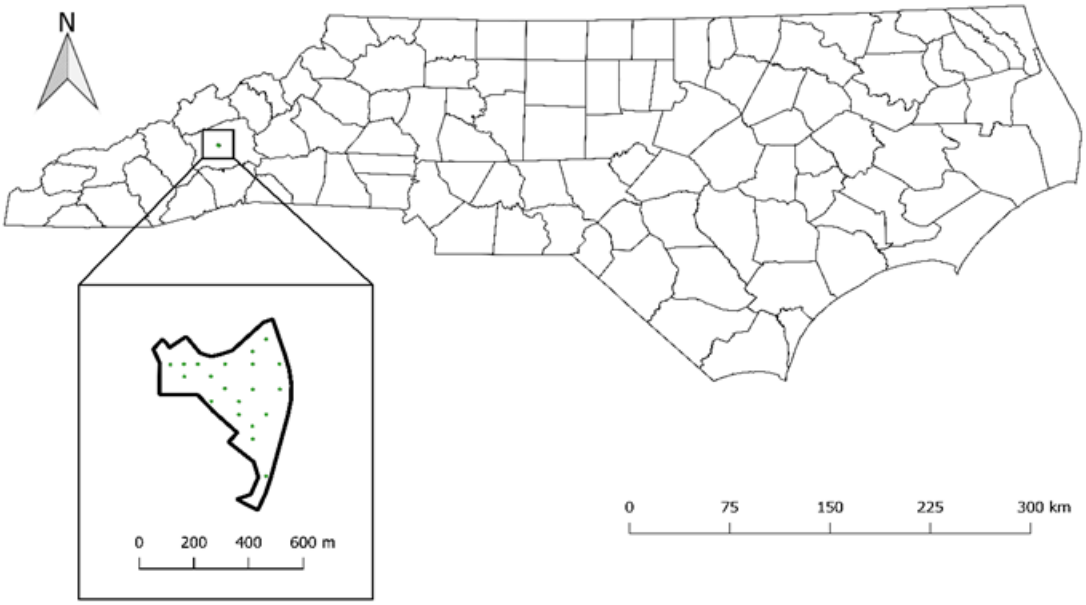


Figure 4.2. Om Sanctuary study site located just outside of Asheville, NC. This was a small site, only covering 42 acres. The green points are the locations of the measured inventory plots.

This location also proved as challenging as the Clinch Mountain site, since it was located on a steep slope, where the land area dropped to the river below, preventing the sUAS from being staged near the study site at the base of the slope. It was preferred to be at the base to maintain proper line of sight (LOS) to the sUAS as it imaged the forest. As with the previous site, these forests were also of the temperate deciduous type, being mostly composed of eastern USA broadleaf trees. A carbon audit was completed at this location in March 2017, measuring all vegetation with DBH larger than 5" (~12.7 cm). Total height was measured, along with models produced of volume, above ground biomass (AGB), total carbon, and AGLC. The areas measured consisted of 20, 0.1 acre (~0.04 ha) fixed-radius plots, measuring 345 individual trees. Only nine plots had tree height values reported, while all other measures and models were produced for all 20 plots. These nine plots contained 149 individual samples.

### 4.4.2 Data Collection

The manned ALS data collection was completed on July 20, 2017 over the Clinch Mountain study site. A commercial vendor was contracted to image the study site with a manned ALS system and Vexcel color (RGB) camera system. A Leica ALS80 small-footprint discrete return lidar, mounted on a fixed wing aircraft, was flown at a constant altitude approximately 7,850 ft (~2,400 m) above mean sea level, and 4,849 – 5,951 ft (~1,478 – 1,814 m) above ground level. This sensor has a scanning rate of up to 200 Hz and a pulse rate of 1 MHz. The point clouds from the vendor included intensity values for the first three returns of each pulse and a return number up to five for each pulse, but point clouds were not classified (ground vs. non-ground). Point densities achieved using this sensor's configuration ranged from 30.44 pts/$m^2$ to 99.16 pts/$m^2$, with an average point density of 71.19 pts/$m^2$. The inconsistency between point density was attributed to the inconsistent overlap of flight paths at the actual plot locations, with the plots towards of the center of the study area receiving the most coverage.

The sUAS ALS data collections were completed on August 11 and 13, 2017 at the Clinch Mountain site and on August 12, 2017 at the Om Sanctuary. The platform used for the sUAS was a DJI Matrice M-600 Pro, with a custom payload rig capable of lifting a modular sensor platform which houses various imagers. For this collection, a weight ballast, lidar sensor and an RGB camera for the SfM section were flown. In this configuration, the sUAS is capable of flying for

approximately 18 minutes. The longest flight completed in this study was approximately 16 minutes and covered three plot locations. For these collects, a Velodyne VLP-16 small footprint discrete lidar was utilized on the sUAS, in combination with a differential GPS/INU system for precise tracking and three-dimensional point cloud generation. This system integration was designed and completed by the UAS Research Lab in the Chester F. Carlson Center for Imaging Science at Rochester Institute of Technology and has been named the MX-1. A depiction of the platform as flown can be seen in Figure 4.3.

Figure 4.3. MX-1 platform developed by RIT. The Velodyne VLP-16 lidar is visible on the forward end of the peripheral mount at the bottom of the airframe.

The flight altitudes above the plots varied from 200 – 300 ft (~60-90 m) above ground level. This was due to the lack of precision in the DEM that the flight software used in terrain following mode. In-flight variations were less than 10 ft (~3.3 m), but the manner by which the flight software set the target height was variable at each location. The VLP-16 lidar has a pulse rate of 300 KHz and a scan rate of up to 20 Hz. The lidar system has a maximum range of 328 ft (100 m), the maximum swath width, assuming -10° to 10° sight lines like that of the ALS80, is 113 ft (~35 m). The VLP-16 is capable of 360° scanning, but it is not recommended to use scans at oblique angles for foliage mapping, as large scan angles may introduce error and occlusions [38]–[40]. The VLP-16 is a two return system, recording the first and last return for every pulse, along with associated intensities. With this system, point densities achieved were 497.04-2,393.93 pts/$m^2$ with a mean point density of 1,504.2 pts/$m^2$. This variance in point density was

attributed the flight altitude, changes in flight overlap from plot-to-plot, and degradation in GPS signal, which resulted in a significant number of returns being removed from the final point cloud. A summary of both lidar system specifications, as flown for both sites, can be found in Table 4.1.

Table 4.1. Lidar sensor specifications as flown for both sites.

| | **Leica ALS80** | **Velodyne VLP-16** |
|---|---|---|
| **Laser Altitude** (ft) | 7,850 | 200-300 |
| **Swath Width** (ft) | 1,800 | 35-52 |
| **Scan Rate** (Hz) | 120 | 10 |
| **Pulse Rate** (KHz) | 1000 | 300 |
| **Returns** | ≤ 5 | ≤ 2 (first and last) |
| **Average Horizontal Resolvable Distance Between Points** (ft) | 4.72 | 1.18 |
| **Footprint** (ft) | 4.02 | 1.57 |
| **Wavelength** (nm) | 1064 | 903 |

Imagery for the SfM portion of the study was collected simultaneously with the lidar data by both platforms. The manned aircraft deployed a four channel, visible and near infrared, Vexcel UltraCam Eagle with a capture scheme of 60% stereo forward overlap between exposures and 30% side overlap between flight lines. The delivered imagery measured a mean size of 24,267 x 21,274 pixels, with a mean GSD of 9 cm at the ground level. The sUAS system deployed an Allied Vision Mako G-419 RGB camera with a capture scheme of 80% forward overlap between exposures and 80% side overlap between flight lines. The delivered imagery measured 2,048 x 2,048, with a mean GSD of 2.5 cm at the ground level. The sUAS utilized a checkerboard fight pattern and image sample rates of 1 Hz to generate high overlap of stereo imagery for generation of high-density lidar point clouds. The manned aircraft used a more traditional flight strip pattern of collection, ensuring that the swaths of each strip overlapped to increase lidar point densities, but did not include specific flight patterns to support SfM efforts. A simple depiction of these two flight paths over a circular target can be seen in Figure 4.4.

Agisoft Photoscan Professional v1.2.6 was used to implement the SfM algorithms for

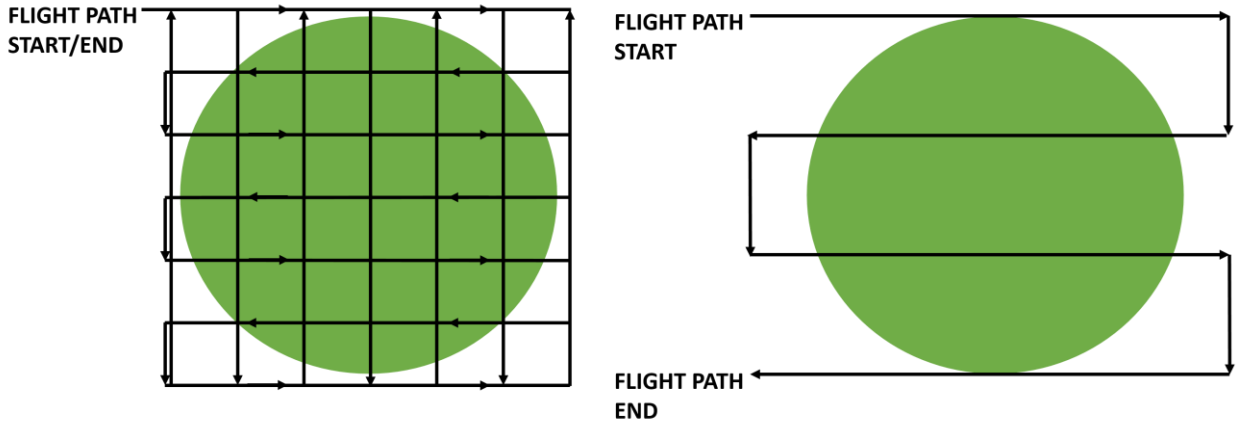


Figure 4.4. Checkerboard flight pattern (left) vs. traditional flight strips (right) over a circular forestry plot outline

these two imagery data sets in order to generate three dimensional point clouds from stereo imagery [64]. In depth details of the processing steps of Photoscan can be found in [31], [32], [65]. A brief overview of the processing flow, is that Photoscan initially detects key point feature matches between the images using a process based on the Scale Invariant Feature Transform (SIFT) [32], [65]. Three dimensional positions of the key points and camera positions are then estimated through an iterative bundle adjustment, and this information is used to generate a dense point cloud from the imagery [36]. In our scenes, ground control points (GCP) were not available for georeferencing the generated point cloud coordinates, thus the direct georeferencing was completed using the GPS information from the system at the time of each image capture. This is the same method used by *Wallace et al.* and *Turner et al.* [32], [36]. An advantage of using this method for georeferencing was that the SfM closely matched the accuracy of the lidar point clouds, since both data sets drew their georeferencing processing from the same source. Throughout the processing workflow of Photoscan, high accuracy settings were used for the alignment of photos, alignment of camera positions, and the generation of the dense point clouds. The final point clouds were exported to the American Society for Photogrammetry and Remote Sensing (ASPRS) ".las" file format to match the lidar data products and for ingestion into the lidar software tools used for processing.

### 4.4.3 Point Cloud Pre-processing

Each lidar data set was delivered in an unclassified format with height values reported in reference to altitude above mean sea level. This required that each data set be processed through a ground classification algorithm for generation of a DEM. The DEM is used to normalize the point cloud to height above ground, rather than altitude above mean sea level. Additionally, a coordinate transformation was completed so that both data sets were represented in the UTM 17N coordinate system. These pre-processing steps were completed using the software suite LAStools, utilizing the function *lasground_new* with a step size of six meters for the ground classification of the point clouds, and the coordinate transformations were completed using the function *las2las* [42].

Square buffers measuring 200 ft. x 200 ft. (60.96 m x 60.96 m), centered on the same locations as the ground reference plots, were developed first to reduce point clouds to the points in the immediate area of interest. This strategy conserved memory and facilitated increased processing speeds by reducing point clouds to manageable sizes for ground classification and normalization, as most files contained >10 million points, for both the lidar and SfM point clouds. Such large buffers avoid edge artifacts on the digital elevation model (DEM) produced, as the ground point classification routine typically contained false positives along the edges of the point cloud. Circular buffers, matching the fixed radius of the reference plots of 37.5 ft (11.43 m), were used for the final reduction of the point clouds. The buffers were generated using the QGIS software package [48]. The clipping, or intersection, of the point clouds with the shape files were completed using *polyclipdata* from the FUSION software suite [20]. A depiction of the processing flow can be seen in Figure 4.5.

The normalization of point clouds was completed using the *lasground_new* or *lasheight* functions from LAStools, depending on whether the DEM was being applied to the lidar point clouds (*lasground_new*) or the SfM point clouds (*lasheight*). The SfM for both data sets failed to generate enough ground returns to generate any sort of reliable terrain map, so a hybrid approach using the DEM generated from the corresponding lidar data sets was required for normalizing the SfM point clouds; this will later be discussed as a distinct disadvantage of the more cost-effective SfM approach.

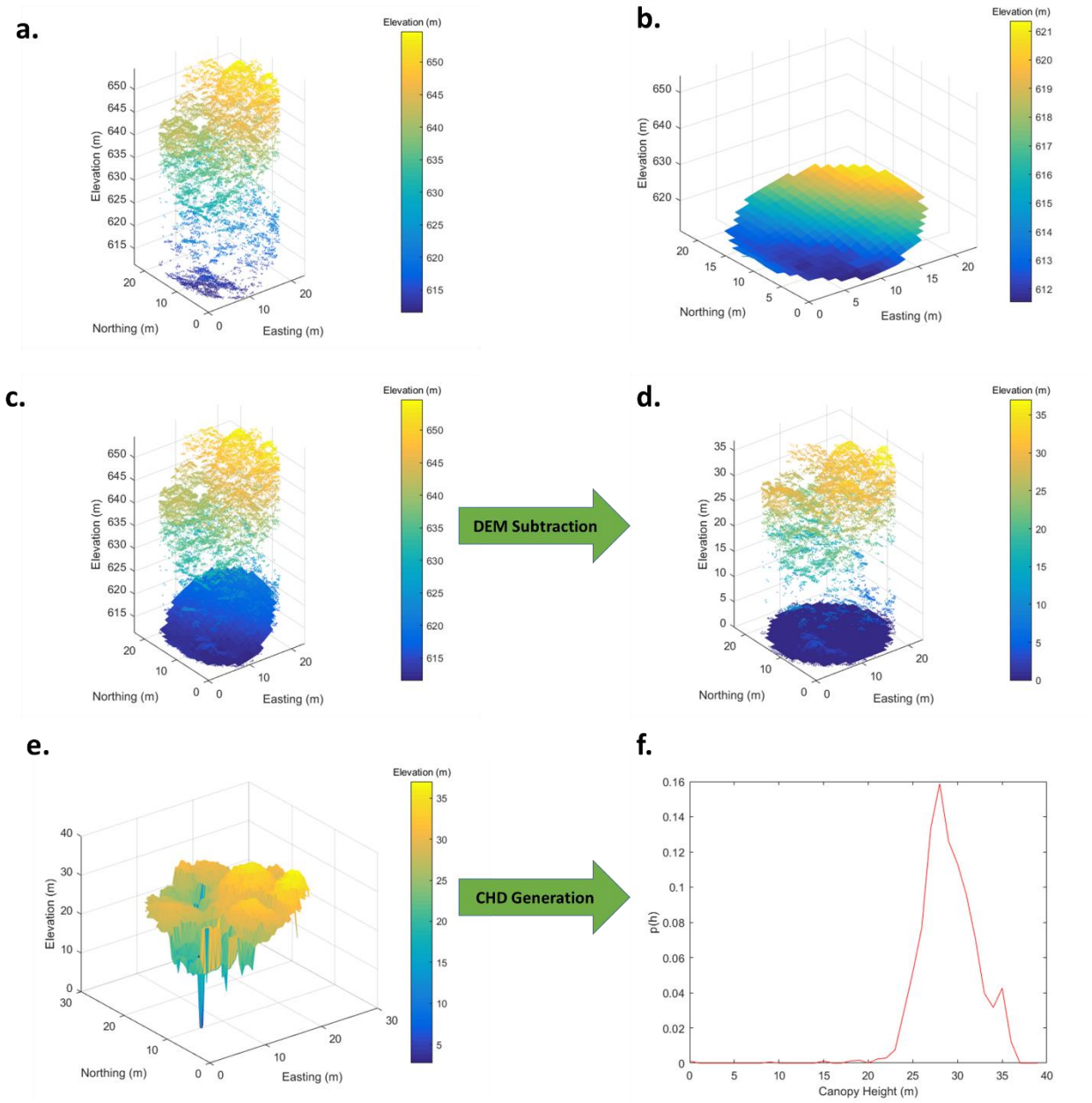


Figure 4.5. Depiction of point cloud processing steps. (a.) Raw point cloud with elevation values referencing mean seal level, (b.) DEM generated from ground-classified points, (c.) Raw point cloud plotted above DEM for visual reference, (d.) Normalized point cloud after DEM subtraction with normalized DEM for visual reference. (e.) CHM generated from normalize point cloud. (f.) CHD generated from the CHM.

### 4.4.4 Functional Carbon Model

A primary metric of concern for sustainable forest management is the measure of carbon stored in the forest, and any changes to that sequestered carbon over time. It therefore is imperative to model these data, as it cannot be measured directly from the remote sensing data. It has been shown that the carbon and AGB relationship can be approximated as a linear function, whereby carbon is approximated as 50% of the biomass value [66]–[69]. This method is common as biomass and carbon can only be directly measured through destructive methods [68]. Assuming this relationship holds true, then a linear AGB model can be trained to create a linear carbon model.

*Zhao et al.* introduced a linear, scale- and shape-invariant, temporally stable model for relating the canopy height distribution (CHD) to biomass density. It is mathematically derived from the allometric relationships of canopy height and diameter at breast height, used by ground crews to generate biomass estimates from field data [58], [63]. Our carbon model is derived from this same framework, since it is a linear model. The model references a data product referred to the authors as the *Canopy Height Distribution* (CHD), denoted as $p(h)$. This can be thought of as the percentage of ground, within the plot being measured, that is obscured by the top canopy at a given height. Effectively the CHD is a histogram of the CHM height values measured at discrete height bins. Since the model is a function of a function itself, it is referred to as a functional model, i.e., the predictor $p(h)$ is function or curve and not a group of predictors [63], [70]. The relationship between the CHD and biomass, or carbon density, can be described by Equation 4.1, with the full derivation from allometric assumptions summarized by *Zhao et al* [58].

$$C_{plot} = f\left(p_{i=1,\dots n}\right) = \int k(h)p(h)dh \xrightarrow{discretized\ by\ \Delta h} \Delta h \sum_{i=1}^{n} k(h_i)p(h_i) \qquad (4.1)$$

where $k(h)$ or $k_{i=1,\dots n}$is a non-negative, non-decreasing function whose value at $h = 0$, is zero. These constraints are derived from the assumption that no forest biomass or carbon is present if there is no canopy, and that forest biomass or carbon increases with increasing height values [58]. For our model, the discrete version of Equation 4.1 is used, setting $\Delta h = 1$ m; this generated $n = 40$ height bins for our data, as the maximum tree height observed was 41.62 m. The fitting of the weighting function $k_{i=1,\dots n}$ was accomplished using the Matlab (ver. R2016b)

function *lsqlin* and applying the constraints detailed previously [71].

A challenge with validating biomass and carbon models from other studies is that each data set covers a different distribution of biomass and carbon, and potentially different forest types. Zolkos *et al.* addressed this issue in their review of 70 published AGB studies and found that expressing the Residual Standard Error (RSE) of a model relative to the mean AGB or carbon value, provides a satisfactory means of comparing studies between different regions with different forest CHM (or height) distributions [49]. The RSE is defined in Equation 4.2 below.

$$RSE = \sum_{i=1}^{n} \frac{|x_{ip} - x_{if}|}{n} \tag{4.2}$$

where $n$ represents the number of observations, $x_{ip}$ represents the predicted value from the model, and $x_{if}$ represents the field measured values of each observation. From this definition RSE(%) is defined as

$$RSE(\%) = \frac{RSE}{\mu_{Carbon}} \tag{4.3}$$

In their review of these studies it was noted that models assessed on temperate coniferous forest exhibited the lowest error rates (mean RSE(%) = 28.7%), when compared to temperate deciduous forest ( mean RSE(%) = 31%) [49]. In the study by Means *et al.*, it furthermore was found that heteroscedasticity existed in their models of basal area and volume, which also affect carbon and biomass models [2]. Their improvement was to model the natural logarithm of these dependent variables, resulting in improved performance, which was also seen with this data set in an earlier study [18].

In addition to the RSE(%) metric, the $r^2$ and RMSE metrics are reported for each model and are defined in Equation 4.3 and Equation 4.4, respectively, where $n$, $x_{ip}$, and $x_{if}$ are defined as they were in Equation 4.2.

$$RMSE = \sqrt{\sum_{i=1}^{n} \frac{\left(x_{ip} - x_{if}\right)^2}{n}} \tag{4.4}$$

$$r^2 = cor\left(x_{ip}, x_{if}\right)^2 \tag{4.5}$$

All CHMs generated in this study used a 0.5 m raster grid for sampling, and assigned the maximum height return as the value for each cell. Each modality produced dense enough point clouds that no interpolation was required for empty cells.

### 4.4.4 Plot Disturbance Detection

The ability to accurately detect harvesting or disturbance of plots would be beneficial when managing multiple forest landowners, thereby facilitating compliance with sustainable forest management principles. Detection of individual harvested trees has been shown in boreal forests with a success rate of 73.4%, utilizing simple differencing of two CHMs taken two years apart [72]. Individual tree detection in closed-canopy, heavily overlapping deciduous forests, such as the sites in this study, is difficult and generally inaccurate. This led us to complete our analysis at the plot level. Rather than examining differences in structural metrics over a period of time, we investigated the ability to detect disturbed forests in a snapshot of time using one data collection. This is effectively a binary classification problem, i.e., the forest is disturbed or not, underscored by an analysis of how well the classifier can differentiate between the two cases using simple structural metrics, at the plot level, for the study sites in question. These structural metrics were derived from the normalized point cloud and from point density values at discrete heights throughout the canopy. The point density values are different from the CHD in that it considers all point values to derive structural information, rather than just the height values of the top canopy. The density values were calculated as the percentage of point returns that fell within each voxel, with each voxel being defined as a 0.5 m x 0.5 m 0.5 m cubed volume. The voxels can be imagined as placing the point cloud onto 0.5 m raster grid, and then proceeding to partition each resulting column of points at standard heights, in this case at every 0.5 m, until the height bins have reached a value larger than the maximum height return in the point cloud. These density values are then aggregated in the $x$ and $y$ directions, to generate a vertical structure profile for the plot as a whole, in terms of the percentage of returns occurring within the associated height bin.

These vertical profiles are analogous to the return type seen in a waveform lidar system and have been used to classify forest change temporally [58]. Considering this, a few metrics were chosen as predication variables:

- The height of the maximum energy, $h_{max}$, an indicator of the height at which the dominant canopy resides, this value is expected to be reduced in heavily disturbed or harvested plots. The calculation of $h_{max}$ excludes ground returns, as it is intended to be a measure of dominant canopy height.
- Height of median energy (HOME), as defined by *Drake et al.*, being the height at which the 50$^{th}$ percentile of returns occurs, was chosen based on its ability to not only consider the dominant canopy as $h_{max}$ does, but it is also affected by the understory [68]. A key difference in the HOME metric in this study when compared to the version that *Drake et al.* implemented, is that values below 1.5 m were ignored for our study to reduce the influence of ground returns on the HOME metric. I.e., we intended for the HOME metric to be indicative of vegetative canopy values. It is noted that the original definition of HOME can be influenced by the ground returns, and indirectly provide insight into gap percentages of plots [69].
- Gap percentage is calculated directly in this study, thus we chose to remove that influence from the HOME metric. The gap percentage was calculated as the ratio of ground returns to total number of returns in a point cloud that contained only the first return value for each pulse [73].

For the binary classification operation, a linear support vector machine was trained using the *fticsvm* function in Matlab (ver. R2016b) [71]. To validate the classifier, two methods were chosen for comparison: holdout cross-validation, where 50% of the observations were used for training and 50% used for validation, and leave-one-out cross validation, where all but one observation was used for training and the remaining observation used for testing [74]. Using these methods, 1000 trials were conducted and the mean value of the Producer's accuracy, User's accuracy, and the Kappa statistic were reported. These two methods of validation were chosen as there were only seven harvested plots in the 49 plot data set, thus fold numbers were limited to seven for leave-one-out cross validation. It was determined that a comparison of the two validation methods would be the most informative of the performance of the classifier in differentiating between disturbed and undisturbed plots, given the small sample size of harvested plots. Although the sample size arguably is of concern for such a complex classifier, the cross-validation approach used here should at least provide a robust indication of performance.

## 4.5 RESULTS AND DISCUSSION

### 4.5.1 Carbon Models

The functional carbon model is derived directly from the CHM, generating the CHD function from the CHM. It was imperative that the generated CHMs are accurate and precise measurements of the forest structure. However, coordinate alignment of the point clouds was one challenge encountered with generating these models. The geographic information system (GIS) shape files, manned lidar data, and sUAS lidar data were all delivered in differing coordinate reference systems (CRS), all of which referenced differing geoids. This introduced alignment errors in initial trials, until the most accurate method of processing was identified as processing point clouds in local coordinates, convert the shape files to the local CRS of each lidar point cloud, and generate CHMs in that reference frame. The shape files should have no altitude component and suffer less error in transformation. Final alignments showed less than 1 m in alignment disagreement between the two data sources, i.e., manned to sUAS ALS. This issue, however, does highlight the advantage of including GCPs in the target scene whenever possible, as there would be reference points to correct for these types of errors. A depiction of example CHMs for each data source can be seen in Figure 4.6.

The manned lidar was the only data set able to cover enough sample plots to generate a truly usable model. The sUAS covered two different study sites, and the differences in species were enough to reduce performance. It was noted by the original authors of this modeling method that the $k(h)$ function in Equation 4.1 is affected by tree allometry and crown geometries, thus, retraining (model calibration) for each new forest type is required [58]. The model performance improved when applied individually to each study site separately; however, sample sizes were small (9-13 samples, depending on sensor) for each site due to loss of data from sUAS timing signal corruption issues during flight. The SfM performance of the manned aircraft collection also was deemed unsatisfactory. Shadowing affects, due to the wide flight lines used to collect the lidar data, precluded many plots from generating full coverage of the study site, thus rendering it unusable for any type of modeling of forest structure or carbon metrics. An example plot showing heavy shadowing is shown in Figure 4.6, panel (b.). The sUAS SfM performance was visibly and quantitatively superior, generating point clouds

densities in the range of 1648.14 – 8826.46 pts/m$^2$, and a mean density of 3,971.71 pts/m$^2$. This was attributed to the checkboard flight path used to generate imagery from multiple view angles of the study site and thereby avoiding shadowing affects. However, neither SfM data set produced adequate terrain measurements and required normalization by the DEMs generated from the lidar point clouds, for their associated sensor platform. The mean difference between the CHM generated by the sUAS lidar and sUAS SfM methods was 1.96 m. The majority of this error was attributed to the boundary "sharpness" with which the SfM methods were capable of generating three-dimensional data, compared to blurring of the sharp edges due to the relatively

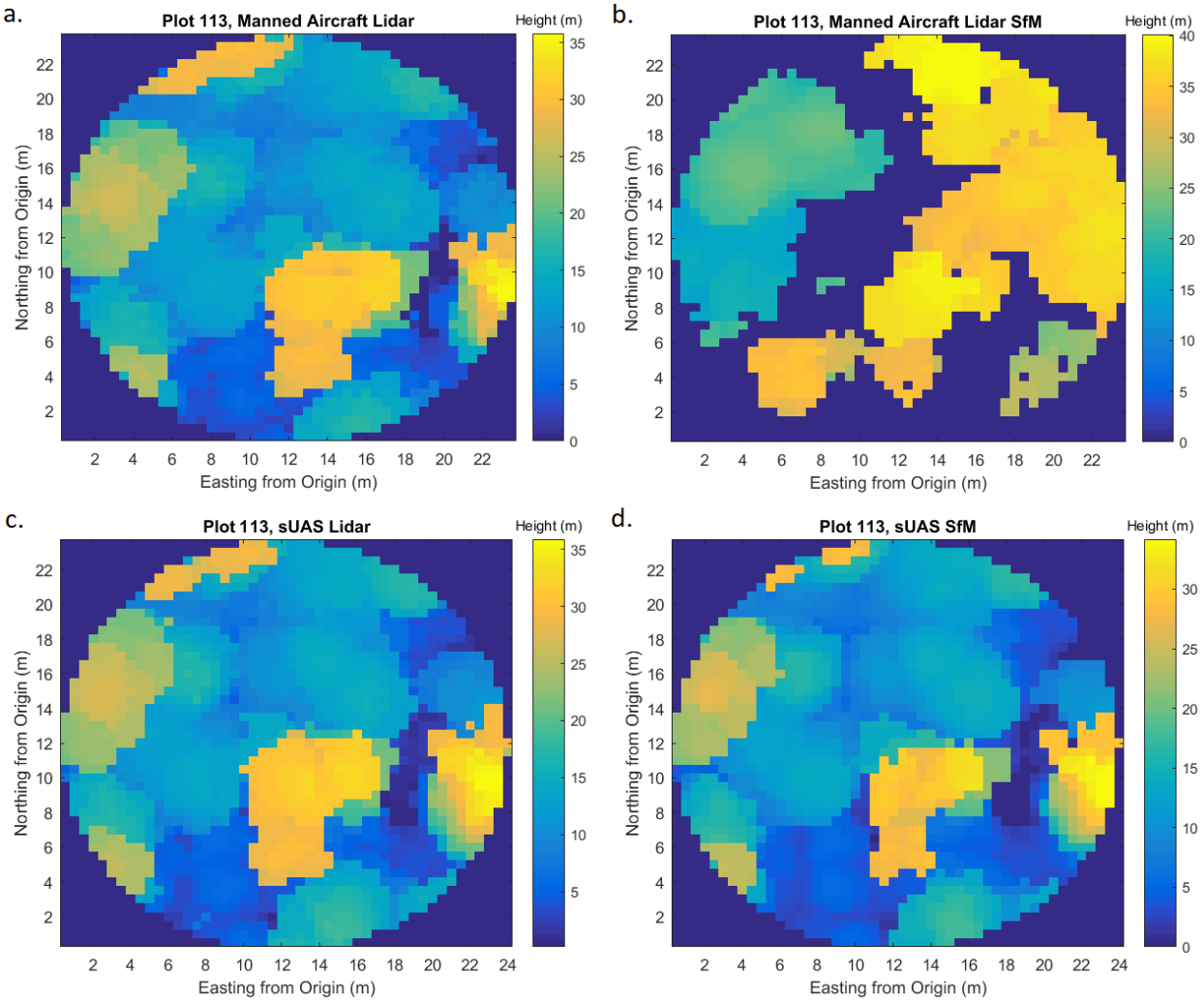


Figure 4.6. Sample CHMs derived from the different sensor modalities of Plot 113, this plot is one of the disturbed plots with high variation in canopy structure. (a.) CHM derived from lidar data set generated by the manned aircraft system, (b.) CHM derived from SfM data set generated by the manned aircraft system, (c.) CHM derived from lidar data set generated by the sUAS, (d.) CHM derived from SfM data set generated by the sUAS.

large footprint of the laser systems. This can be seen in Figure 4.6, panel (c.) and (d.); plot 113 contains large magnitude, high frequency changes in canopy height, the lidar-generated CHM has a blurring of these edges when compared to the SfM-generated CHM. All CHMs in this study were generated on the same 0.5 m raster grid.

The manned airborne system's lidar data performed well when modeling the logarithm of the carbon data ($r^2 = 0.64, RMSE = 17.14$ Mg C/ha $RSE(\%) = 27.83\%$), falling just short of the performance of the model when applied to a coniferous forest by the original authors ($r^2 = 0.72, RMSE = 10.75$ Mg C/ha) [63]. This is a positive result, as it is common for biomass and carbon models to exhibit worse performance in deciduous forests, achieving lower $R^2$ values and larger RMSE values than for coniferous sites [75]. Additionally, the RSE(%) attained is below the average RSE(%) reported by *Zolkos et al.* for models applied to this forest type [49]. The full lidar data set for the sUAS resulted in poor results ($r^2 = 0.12, RMSE = 21.72$ Mg C/ha $RSE(\%) = 49.73\%$), stemming from the species and forest structures differences between the two study sites. The results of each model application can be found in Table 4.2.

In order to complete a comparison of the manned to unmanned platforms, two methods were chosen. It should be noted that when the modeling was applied separately to the VA data or the NC data, performance improved dramatically to $r^2 = 0.70, RMSE = 10.02$ Mg C/ha, $RSE(\%) = 19.35\%$, and $r^2 = 0.82,\ RMSE = 3.01$ Mg C/ha $RSE(\%) = 11.33\%$, respectively. The first method explored was to reduce the manned lidar data set to only first and last returns, simulating the sampling scheme that the sUAS lidar employs. This method resulted in identical results, as expected, considering the CHM is generated by a majority of first returns, since the first returns typically contain the maximum value for each grid cell. The second method was to apply the sUAS CHD functions, generated from the four plots that overlap between the manned aircraft and sUAS data, to the manned aircraft trained model. The predictions for these plots closely agreed between the two data sets, with $r^2 = 0.99, RMSE = 1.77$ Mg C/ha. This demonstrates that both systems are capable of producing similar predictions when imaging the same study sites and not suffering from component failure.

Table 4.2. Carbon model results. All models were fit to the $\ln(C_f)$, where $C_f$ is the field measured carbon data by the ground crew during the audit.

| Sensor Platform | Data Source | Number of Samples | Returns | $r^2$ | RMSE (Mg C/ha) | RSE (Mg C/ha) | RSE(%) |
|---|---|---|---|---|---|---|---|
| Manned Aircraft | Manned Lidar | 49 | All | 0.64 | 17.14 | 13.08 | 27.83 |
| | Proxy sUAS Lidar | 49 | First and last | 0.64 | 17.14 | 13.08 | 27.83 |
| | Proxy manned aircraft SfM | 49 | First Only | 0.64 | 17.14 | 13.08 | 27.83 |
| sUAS | sUAS lidar, All plots | 19 | All | 0.12 | 17.86 | 21.72 | 49.73 |
| | sUAS lidar, VA only | 10 | All | 0.70 | 11.31 | 10.02 | 19.35 |
| | sUAS SfM, VA only | 13 | All | 0.68 | 12.55 | 10.51 | 21.90 |
| | sUAS lidar, NC only | 9 | All | 0.82 | 3.01 | 2.10 | 11.48 |
| | sUAS SfM, NC only | 9 | All | 0.84 | 2.83 | 2.07 | 11.33 |

The SfM data from the sUAS underwent a similar testing procedure of applying the SfM CHD to the trained manned carbon model, as the sUAS SfM model suffered from the same issues between the two study sites as the lidar data. When investigating the four overlapping plots, similar performance was found to those from the lidar comparison, namely $r^2 = 0.98, RMSE = 2.13$ Mg C/ha, indicating that a hybrid approach of lidar-derived DEMs and SfM-generated CHDs is a viable option. The manned SfM failed to produce usable data; a proxy data set was generated in lieu of this to simulate low-density SfM point clouds from the manned lidar data. The manned lidar data were reduced to first returns only, as it was noted that no ground measurements were made by the SfM methods due to the dense canopy obscuring views of the underlying terrain. Again, as with the previous proxy data set, the results were identical to the manned lidar model for the same reasons, given that the highest elevation returns have the strongest influence on the CHDs. This presents an opportunity for a large cost savings, as obtaining and operating a RGB camera is significantly more affordable than lidar sensor packages. Considering that the underlying terrain does not shift often in these areas, a concept of

operations would be to source a lidar collection for creation of high quality DEMs and use SfM at later dates to collect canopy structure measurements, even for temporal (change detection) analyses.

### 4.5.2 Detecting Plot Disturbance

Plot disturbance, to include natural events such as wind and storm damage, or harvesting, was considered a proxy for assessment of "forest sustainability", i.e., to identify exploitative harvesting practices. This would enable an approach to gather information related to compliance with sustainable harvesting principles. The Montreal Process has identified seven indicators that are directly or indirectly related to change detection of carbon levels in forests, such as total forest ecosystem carbon pools and fluxes, total growing stock, annual increment in species available for wood production, fragmentation levels of forests etc. [16]. To support this type of effort, we proposed to classify vertical distribution data at the plot level, derived from lidar voxels, as the lidar systems are the only modality that generated returns for the underlying or sub-canopy vegetation structure. The sUAS lidar did not cover enough examples of disturbed forest to be used for training and testing of a classifier, thus the data from the manned lidar system was used exclusively for this purpose. The structural data generated from the voxels have been shown to be capable of discriminating between varying stand types over time [63]. Rather than look at change detection over time, we explored the ability of the structural data to discriminate between potential harvested forest plots. A plot of the generated vertical profiles for all stands, disturbed and undisturbed, and a depiction of only the disturbed stands can be seen in Figure 4.7. A graph illustrating the mean vertical profile of each class of plot can be referenced in Figure 4.8.

We explored the use of binary classification to label plots as disturbed or undisturbed. Three structural metrics were chosen for use as feature descriptors. The features chosen from the previously mentioned seven viable indicators were: height of maximum energy, $h_{max}$, an indicator of dominant canopy height, height of median energy, HOME, and the gap percentage of each observation. Height of maximum energy, corresponding the dominant canopy height, is a logical choice for this classifier, since a more heavily harvested forest, i.e., a forest that is in non-compliance with sustainable forest management principles, will have a significantly shorter

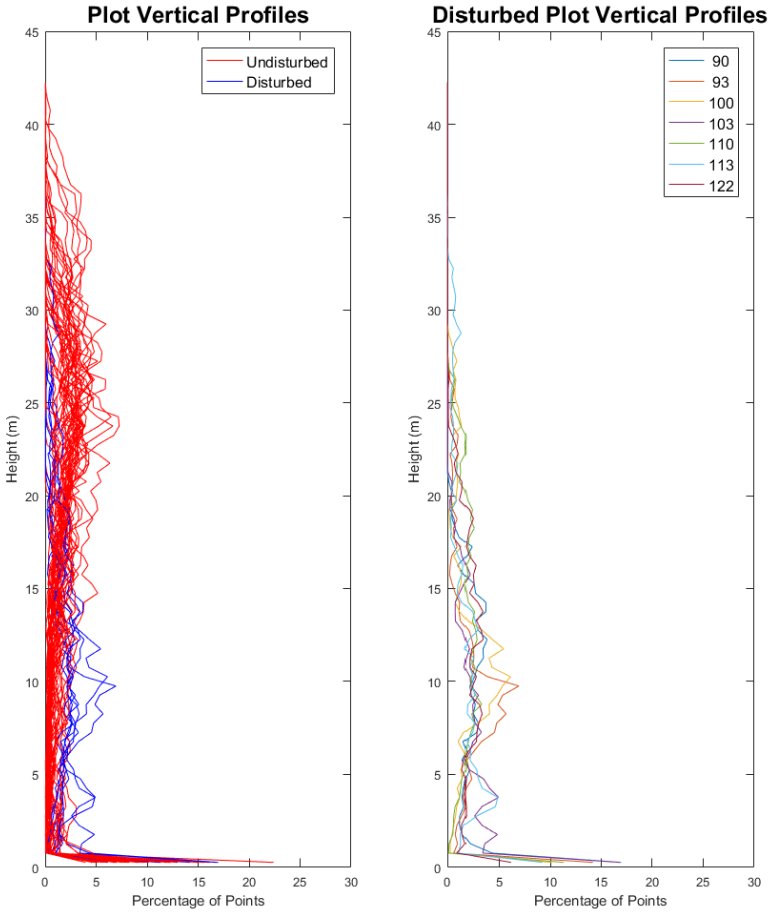


Figure 4.7. Vertical profiles of each forest plot generated from voxel point-density measurements. The left pane shows the disturbed and undisturbed vertical structure profiles, the right pane shows only the disturbed plots, to enable direct inspection of the structural details of these disturbed plots.

canopy than an undisturbed forest, and has been noted to show variation based on treatment methods of plots during growth [76]. HOME has been shown to be sensitive to underlying vegetation cover, and has provided high levels of predictive power in the variability of between plots [68], [69]. Visualization of $h_{max}$ and HOME for the mean vertical structure of the disturbed and undisturbed forest can be seen in Figure 4.8. Note the clear differences in the vertical profiles and the inverted relationship between HOME and $h_{max}$ in the disturbed observations. As larger sections of vegetation is harvested or damaged by natural events, an increase in canopy gaps is expected, thus this variable was also included.

A linear SVM generates a linear decision boundary between two groups of data points. This is achieved by attempting to maximize the margin between the decision boundaries and the

neighboring data points [77]. We chose three feature descriptors of our data set, thus, the decision boundary is a two-dimensional plane, and it would be a simple line for a two-dimensional feature set. An example of one of many generated decision boundaries in this study can be seen in **Error! Reference source not found.**. The SVM will generate a different decision boundary for each set of inputs, requiring multiple repeated trials to gain insight into the average performance of the classifier. In this study, the data set is clearly linearly separable, with many of the training sets yielding similarly oriented hyperplanes. These properties allowed for the development of a high performing classifier.

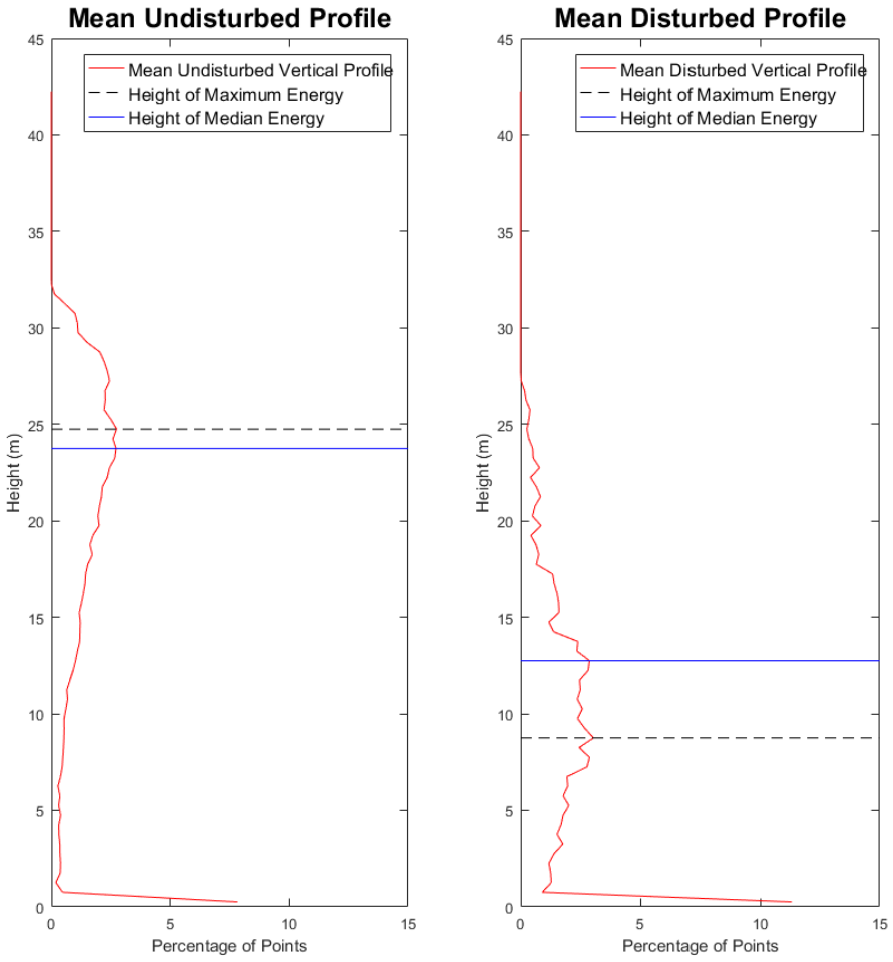


Figure 4.8. Mean vertical profiles for undisturbed observations (left) and disturbed observations (right). HOME and $h_{max}$ for each are depicted by the blue line and black dashed line respectively.

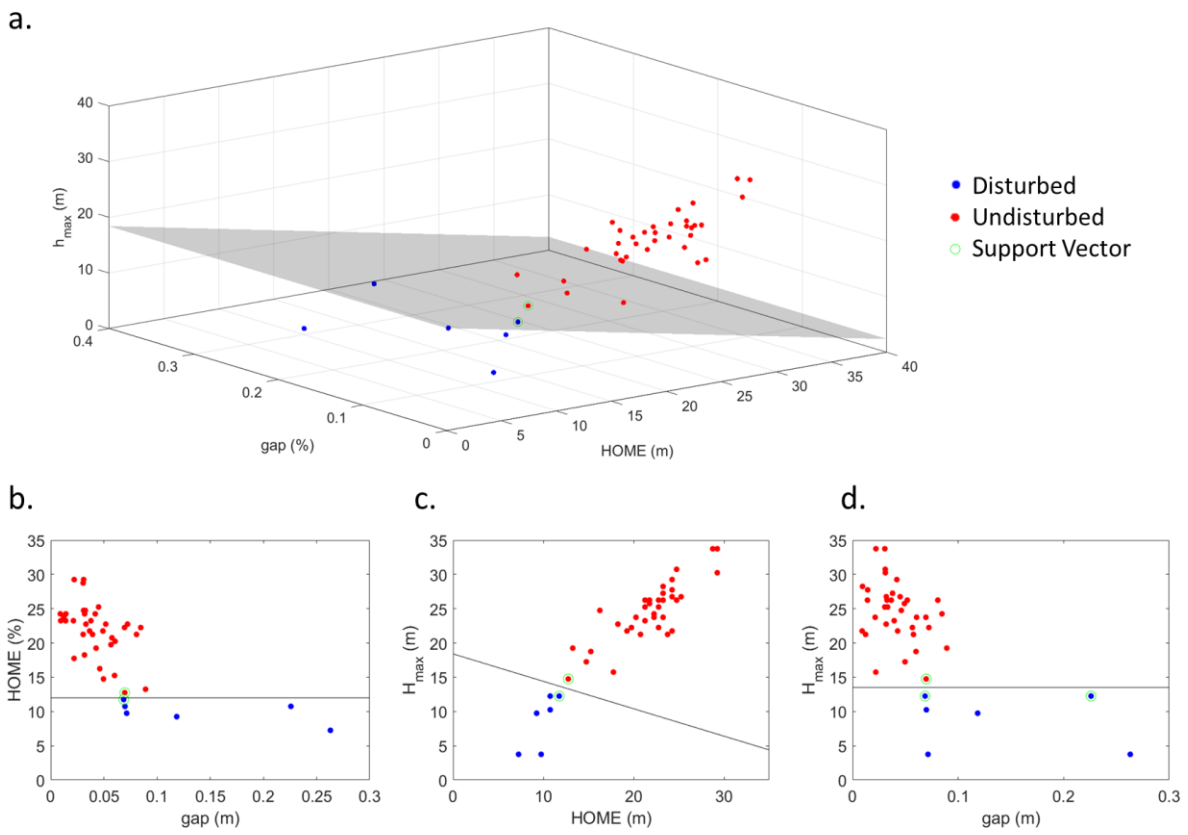


Figure 4.9. (a) A depiction of the feature descriptors and decision plane in three-dimensional space. (b – d) Two-dimensional depictions of feature descriptors and possible decision boundaries, for the HOME vs. gap (b), maximum height vs. HOME (c), and maximum height vs. gap (d) variable sets.

Two validation methods were used to test the classifier's performance on the data set. This data set is highly unbalanced with seven samples for the disturbed class and 42 samples for the undisturbed class. The first validation method chosen was leave-one-out cross validation. We use the leave-out phrase in reference to the disturbed training class, meaning that the data set as a whole is split into seven stratified folds, utilizing six folds for training and one fold for testing. This method yielded training sample sizes of six disturbed samples and 36 undisturbed samples, while the test fold contained the one remaining disturbed observation and six remaining undisturbed samples. This type of validation scheme resulted in highly accurate classification rates over 1000 iterations. The Producer's, User's accuracy and the Kappa statistic for the disturbed class with this validation method were 100%, 99.1%, and 99.2%, respectively. The classifier performed very well on average, however, there were large variances in the User's accuracy, with the Kappa statistic noting a lack in preciseness of the detector. The large variances was attributed to the small sample size of the disturbed class, with every false positive

and false negative resulting in a large change in measured accuracy. This is illustrated by the fact that the performance metrics for the undisturbed class were much less affected by these errors, as seen in Table 4.3.

The second validation method chosen was a stratified random holdout cross validation, where the sample distributions were split in half by class, disturbed or undisturbed. This resulted in 21 samples for the undisturbed plots in the training and test folds, while the disturbed plots alternated between three and four samples for the training and test folds. This method resulted in a reduction of performance across all metrics, from a reduction in mean accuracies to an increase in variances, but performance was still high. The Producer's, User's accuracies, and the Kappa statistic for this validation method were 94.1%, 92.2%, and 89.8%, respectively. These reductions in performance were attributed to the reduced training instances to train the classifier, however, we feel that this validation method presents a more rigorous test environment considering the unbalanced data set at hand. This method also suffered from the large variance issue that plagues the first method, due to the small sample size of the disturbed class.

We expanded the disturbance or non-sustainability detection to also include plots with moderate harvest conditions, 10 years prior to the collection date. These moderate disturbances proved to be difficult for the classifier to identify and were not clearly separable via the structural features we had chosen to use for our methods. This can be seen in an example of the hyperplane

Table 4.3. Results of disturbance detector method. The detector performed best when applied to the aggressively harvested plots, but performed poorly when applied to all disturbed plots.

| Data Set | Validation Scheme | Class | Prod. Acc. | User Acc. | Kappa |
|---|---|---|---|---|---|
| Aggressive Harvesting | Leave-one-out | Undisturbed | 99.5% (66.7% - 100%) | 100% | 99.2% (36.4% - 100%) |
| | | Disturbed | 100% | 99.1% (33.3% - 100%) | |
| | Hold-out 50% | Undisturbed | 98.0% (81.0% - 100%) | 99.1% (91.3% - 100%) | 89.8% (46.7% - 100%) |
| | | Disturbed | 94.1% (33.3% - 100%) | 92.2% (42.9% - 100%) | |
| All Harvesting | Leave-one-out | Undisturbed | 84.2% (56.3% - 100%) | 75.0% (57.1% - 100%) | 38.0% (0% - 73.3%) |
| | | Disturbed | 46.0% (0% - 88.8%) | 63.0% (0% - 100%) | |
| | Hold-out 50% | Undisturbed | 84.4% (50% - 100%) | 75.5% (60% - 100%) | 38.5% (0% - 80%) |
| | | Disturbed | 47.5% (0% - 100%) | 63.5% (0% - 100%) | |

generated by the detector while operating on the entire data set, depicted in Figure 4.10, as well as noting the similarities in mean feature values between the undisturbed and moderately disturbed plots in Table 4.4. Many of the moderately disturbed observations are not separable utilizing these structural metrics, as they cluster within much of the undisturbed data points. This is due to the lack of aggressive harvesting which in turn reduced the canopy variation, while also not introducing any large gaps in the canopy. It is worth noting that, in general, the gap feature did not provide as much insight into disturbance classification as HOME and $h_{max}$. This is likely due to the mixed nature of the forest as a whole: When larger vegetation is removed, the understory remains and prevents the first return of the laser pulse from reaching the ground and registering as a gap location.

We conclude, based on these results, that i) given the set of disturbance indicators, the disturbance detector/classifier was capable of reliably detecting heavily disturbed plots and could provide utility in locating interest points for inspection and ii) when the moderately harvested plots were included in the algorithm, the detector performance dropped significantly. This implies that the simple structural features derived from the forest structure, while they have a history of providing insight to other predictive models, were not separable for all harvest instances and severities. Exploration of more intricate structural features or non-linear classification methods may improve results. However, in the context of sustainable forest management, the detector was successful is detecting those plots with the most severe loss, as can be seen by the decision boundary shown in Figure 4.10. Such severe disturbance arguably is representative of top-cutting or even aggressive timber removal practices, both of which could indicate a reduction in forest sustainability.

Table 4.4. Mean feature values for each class of observation.

| **Plot Category** | **Mean $h_{max}$ (m)** | **Mean HOME (m)** | **Mean Gap Fraction (%)** |
|---|---|---|---|
| **Heavily Disturbed** | 8.68 | 10.32 | 12.5% |
| **Moderately Disturbed** | 22.45 | 19.80 | 4.4% |
| **Undisturbed** | 25.5 | 22.55 | 4.6% |

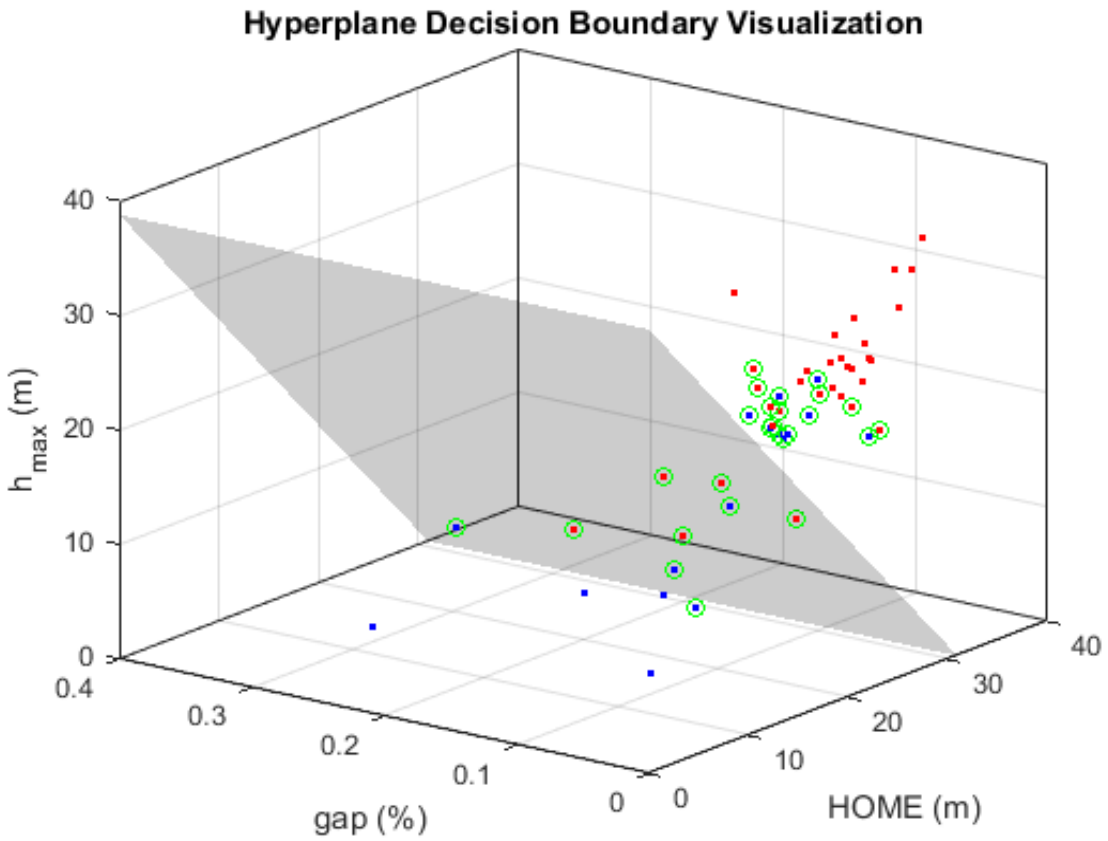


Figure 4.10. Example decision plane generated by the linear SVM when applied to full extent of disturbed observations, including both severe and moderate harvest situations. The large number of support vectors is an indication of a poorly conditioned data set with high rates of confusion. The gray plane is the decision boundary generated by the linear SVM, and the points circled in green are the support vectors.

## 4.6 CONCLUSIONS

This paper had two primary objectives: i) implement a comparison of carbon modeling, derived from sUAS and manned airborne structural data products, utilizing data of a dense heterogeneous deciduous forest located in the southeastern portion of the United States (USA), and ii) evaluate a disturbed, or harvested, plot support vector machine detection method to aid in mapping potentially harvested sites as means for ensuring compliance with sustainable forest management principles. Both lidar and SfM data products were produced for both platforms over deciduous forests in the southeastern USA, including a unique lidar and unique SfM data set for each platform for use in the functional carbon model. The disturbance detector was implemented

as a binary classifier using descriptions of the vertical distributions of each plot from voxels obtained by the ALS systems as features.

The comparison of data sources was completed by implementing a functional model described by *Zhao et al.* to generate a carbon model of each plot measured by both platforms [58], [63]. Initial indications were that both data sets were of high quality, exhibiting high point densities over the study sites. The manned lidar system produced point cloud densities ranging from 30.44 - 99.16 pts/m$^2$, with an average point density of 71.19 pts/m$^2$. However, the SfM method applied to the manned system failed to generate adequate point clouds, suffering from significant shadowing, which in turn obscured tie points needed to generate of 3D coordinates over the measured canopies. The sUAS lidar and SfM methods produced the most dense point clouds, ranging from 497.04-2,393.93 pts/m$^2$, with a mean point density of 1,504.2 pts/m$^2$, and 1648.14 pts/m$^2$ – 8826.46 pts/m$^2$, and a mean density of 3,971.71 pts/m$^2$, respectively.

The manned lidar produced an acceptable performing model, similar to other models developed for deciduous forests ($r^2 = 0.64, RMSE = 17.14$ Mg C/ha $RSE(\%) = 27.83\%$). Only four measured plots overlapped between the manned data collection and the sUAS data collection, due to a data corruption issue (a timing mismatch between the various sUAS data streams). Two proxy data sets therefore were generated from the manned lidar, a set containing first returns only, and another containing both first and last returns; these proxy data sets simulated the manned SfM and sUAS lidar, respectively. The data from the sUAS lidar and SfM methods were ingested into the trained model generated by the manned model. Both inputs produced carbon predictions that closely agreed with the manned lidar data, at $r^2 = 0.99, RMSE = 1.77$ Mg C/ha and $r^2 = 0.98, RMSE = 2.13$ Mg C/ha, respectively. Even though four samples constitutes a small sample size, we concluded this was an indication that the data products generated by each platform, manned and sUAS, were similar and that for small area usage the sUAS is a viable alternative to the manned system, as it also has been shown to be economically competitive [18]. More importantly, this showed for models that rely on CHM, the more affordable method of using SfM methods to generate point clouds is a viable option, if a quality DEM is available for the study site.

The disturbance detector was envisioned as a tool to help land managers flag areas of interest, defined as areas that have been disturbed, whether by natural or man-made means. The

manned lidar was used for this effort, as this data set contained up to five returns per pulse and covered the largest sample sizes of each class type. A linear SVM was used as the binary classifier, operating on features derived from the vertical structure of each plot, calculated from point densities of 0.5 m voxels and aggregating those voxels at each height level. The three features generated from each plot were the height of maximum energy, height of median energy, and gap fraction. All three have been shown to have predictive power in biomass and basal area modeling, and are sensitive to canopy changes [68], [78]. Detection of the heavily disturbed plots generated the following performances for Producer's, User's accuracy, and Kappa statistic: 100%, 99.1%, and 99.2%, respectively, for leave-one-out cross validation; and 94.1%, 92.2%, and 89.8%, respectively, for hold-out cross validation using a 50% ratio between training and test sets. When moderately disturbed plots were introduced in the classifier, detector performance fell drastically, since these plots exhibited similar features to undisturbed plots. It was concluded that features of higher complexity or non-linearity need to be explored for detection of these types of forest, and perhaps the investigation of a multiclass detector.

Overall, this paper met both objectives, albeit with caveats. The sUAS data that did overlap with the manned lidar system performed well in the context of carbon modeling, however, a loss of 50% of the overlapping data (four of eight plots) due to data corruption highlight a strong need to develop system maturity. This system maturity must be attained to develop the sUAS as a viable and reliable alternative to the manned system. Additional challenges to sUAS collections were the FAA line of sight requirements. Navigating dense forests on steep mountainsides creates difficulty in maintaining a visual on the flight operations. Future considerations could include the construction of temporary or permanent towers to raise the vantage point or having multiple safety spotters available for assistance. In the context of the second objective, the detector worked well in detecting heavily disturbed plots, but struggled with moderately disturbed plots. Recommended future improvements would be to generate more intricate descriptions beyond the three structural indicators used in this study. Metrics such has height to living crown, or inspection of the width of the dominant canopy peaks within the vertical structure, could provide insight into the variation of canopy heights within the dominant lobe. This would tie back to harvests completed with sustainable forest management in mind, where clear cuts tend to be avoided.

# Chapter 5

# Summary

## 5.1 SUMMARY

Chapter 1 of this thesis introduces a basic background of sustainable forest management and the role remote sensing has played in increasing our measurement capability for forests. Sustainable forest metrics are introduced, such as stable volume, biomass, carbon and stems-per-hectare (SPHA). The objectives of the thesis also are presented: i) Assess the extensibility of light detection and ranging (lidar) algorithms for forest height, volume, and carbon assessment to UAS platforms and data, ii) Evaluate the use of more cost-effective imagery-based (stereoscopic structure-from-motion) vs. lidar-based algorithms for forest structure assessment, iii) Develop and evaluate a framework for disturbance detection within forest canopy structures, and iv) Publish and present research findings to achieve broad industry dissemination, especially among forest management entities such as the Forest Stewardship Council (FSC) and Rainforest Alliance.

Chapter 2 continues the background of lidar applications, specifically pertaining to sUAS applications within sustainable forest management. This thesis was written in a modern format, where Chapter 3 and Chapter 4 are stand-alone research papers. The background in Chapter 2

thus contains pertinent information that was beyond the scope of the later chapters. This chapter also includes a background on lidar basics for point cloud generation, an overview of the CIS research sUAS, and an overview of the required preprocessing of the data to complete analysis.

Chapter 3 introduces the first comparisons completed using the manned lidar data and sUAS data. This chapter is a slightly modified version of the paper presented at the SPIE Commercial + Scientific Sensing and Imaging, April 2018. A linear regression carbon model is developed for each data set to compare performance and it is determined that each system performed similarly. A cost analysis is presented for context of the economic impact of generating a lidar product for each system. It was found that the sUAS was competitive in cost per area of coverage, but was most suited for small land-area collections.

Chapter 4 introduces a more robust carbon model, the structure-from-motion data sets generated in this study, and the concept of a disturbance detection algorithm. This chapter has not been published at the time this thesis was written, but is written with the intent to submit for publication in a peer-reviewed journal. Similar to the findings in Chapter 3, the carbon model developed here shows agreement between the manned lidar and sUAS lidar data sets. There is also good agreement between the manned lidar and sUAS SfM data set, indicating potentially significant cost savings on sensor acquisition when developing a sUAS for sustainable forest management purposes. The disturbed plot detection methods performed well on heavily disturbed plots, but struggled on moderately disturbed plots. This indicates a potential for detection, but improvements in robustness must be explored.

## 5.2 CONCLUSIONS

Sustainable forest management practices are receiving renewed attention in the growing effort to make continued, efficient use of natural resources. Sustainable management approaches require accurate and timely measurement of the world’s forests to monitor volume and biomass levels, as well as changes in sequestered carbon. It is in this context that remote sensing technologies, which possess the capability to rapidly capture structural data of entire forests, have become a key research area. Sustainable forest management relies on the acquisition of timely and accurate information of the forest. Lidar remote sensing platforms provide the capability of rapid collection with high spatial resolution. The increasing performance

capabilities and reduction of cost associated with small, unmanned aerial systems (sUAS), coupled with the decreasing size and mass of lidar sensors, provide the potential for a cost effective alternative. This drove our research objectives to compare the utility of these sUAS platforms and sensors to that of the standard manned aircraft collections

The evaluated data sets were collected by both types of sensors in the deciduous, mixed-age forests of southeast USA. A simple carbon model was developed for these data sets as a means to compare performance in the sustainable forest management context. Both systems produced adequately dense point clouds, with the manned system exceeding 30 pts/$m^2$ and the sUAS exceeding 400 pts/$m^2$. Both sensors performed similarly in the carbon model with their RSE(%) being within one percent of one another. Having established that the sUAS can produce similar quality models of sustainable forest metrics, a cost analysis was completed of the two data collections. This led to the conclusion that the sUAS is competitive with the manned aircraft at a cost of $8.12/acre, compared to the manned aircraft's cost of $8.09/acre, the latter which excluded mobilization costs of the manned system.

A functional carbon model then was developed with the intent to train with lidar data from the manned aircraft and test on the sUAS data. The trained manned aircraft model performed well, and in line with other models developed for heterogeneous deciduous forest ($r^2 = 0.64, RMSE = 17.14$ Mg C/ha $RSE(\%) = 27.83\%$). A proxy data set, simulating SfM data with first returns, and sUAS lidar data with first and last returns, yielded identical results. The functional model used for the carbon prediction was derived from CHMs, which are highly influenced by the first returns in a 3D point cloud. The four overlapping plots between the sUAS and manned aircraft were used for a direct comparison. The sUAS lidar and SfM both were normalized by a DEM generated from the sUAS lidar, and were ingested into the trained manned aircraft model. This resulted in a high agreement in their predictions, compared to that of the manned data. The error for the sUAS lidar and SfM data were $RMSE = 1.77$ Mg C/ha and $RMSE = 2.13$ Mg C/ha, respectively.

These results, coupled with the results of the first carbon model, led us to the conclusion that the sUAS is capable of generating model performance similar to the manned system. Additionally, we concluded that the SfM data, in a hybrid approach using an externally generated DEM, is a viable alternative solution to a solely lidar-based collection. The SfM point cloud

provide significantly higher point densities and finer detail of the canopy structure. Both of these conclusions directly support our first and second objectives. The publication that Chapter 3 is based on directly supports our fourth objective, along with the publication of this thesis and the intent to publish the research presented in Chapter 4.

We completed another study to further explore relationships of structural canopy data and sustainable forestry applications to support our third objective. A disturbance detector was developed with the intent to draw attention to potentially harvested plots or plots damaged by natural events, e.g., wind or fire damage. The detector was built on a binary classification scheme using a linear SVM and input features of height of maximum energy, height of mean energy, and gap fraction. The first two metrics were based on aggregated point density values derived from 0.5 voxels. This detector performed remarkably well on heavily disturbed plots, generating the following performance measures for detection of disturbances using leave-one-out and holdout cross validation: Producer's, User's accuracy, and Kappa statistic values of 100%, 99.1%, and 99.2%, and 94.1%, 92.2%, and 89.8%, respectively for the leave-one-out and holdout cross validation approaches. However, when incorporating more moderately harvested sites, the detector suffered a drastic decrease in performance. The performance values fell to below 50% for Producer's accuracy and below 65% for User's accuracy, while the Kappa statistics dipped below 40%.

We concluded that the heavily disturbed plots, i.e., the plots that are managed in a potentially unsustainable manner, were successfully detected and the tool would be useful for indicating the presence of these types of sites, as they were still accurately classified, even with the poorer performing version of the tool. As this is the first iteration of the detector, there is always room for improvement. Future implementations should consider metrics that are closer aligned to the variation in the canopy structure. A possible improvement could be to analyze the vertical width of the dominant canopy as a potential description for the selectively harvested plots. These plots would allow more returns from the canopies just below the dominant, thus widening the Guassian-like curve located at the height of maximum energy. Overall, this portion of the thesis was successful in detecting the original, seven heavily disturbed plots given in the reference data.

## 5.2 FUTURE WORK AND IMPROVEMENTS

A few potential future research studies to improve on what was presented in this thesis have been identified, with a focus on potential improvements to flight planning to allow for greater area coverage per flight. These potential studies are contained in the list that follows:

- Our primary driver for the low flight speeds was to limit motion blur in the RGB imagery during data collection. This was a concern due to the low flight altitudes required to accommodate the lidar system. The mean GSD at the terrain level for the collections in this study was 2.5 cm, and the mean GSD at the canopy level, assuming an average canopy height of 30 m, was 1.5 cm. The mean exposure time for the collections was 4.56 ms, resulting in blur levels of 0.36 pixels and 0.59 pixels at the terrain and canopy levels, respectively, which imply relatively low levels of blur. A future study could evaluate the effects of GSD and blur levels on the resulting SfM point clouds and derivative products, e.g., DEMs and CHMs. The objective of such a study would be to investigate potential flight speed increases and the resulting increase in blur levels, and to investigate higher altitude flights, thereby allowing larger areas to be imaged and a potential decrease in blur levels, while increasing GSD. The expectation is that the fine detail generated in this thesis research is not required to generate the DEMs and CHMs, as 0.5 m raster models produced adequate results. Increases in flight altitude and flight speed would allow for larger area coverage per flight, reducing the cost of deployment for the sUAS.

- SfM considerations required for significant overlap in flight lines and low flight speeds. This resulted in extremely high density lidar point clouds. A potential future study could investigate higher flight speeds, while utilizing lower overlap between flight lines, with the intent to generate point densities in the range of which were generated by the manned lidar system. These point density levels were adequate for DEM and CHM generation, which were the key data products utilized for carbon modeling and disturbance detection. By increasing flight speeds and reducing overlap, the point densities would be reduced, but the

coverage area capabilities would increase. This would further reduce the cost of deployment of the sUAS system to levels below the manned system.

- The functional carbon model utilized CHDs generated from CHMs. The CHMs only provide information on the top canopy surface, as they only retain the maximum height value within each raster grid cell and do not utilize structural information of the underlying vegetation. A potential improvement could focus on leveraging the structural information found in the plot point-density waveforms, generated for the disturbance detector through the voxel method. These waveforms capture information about the underlying vegetation structure, potentially providing additional descriptive inputs to the functional carbon model.

In addition, a few improvements in the research approach were identified during the course of this study. These improvements are contained in the list that follows:

- When imaging a scene, whether it is with an electro-optical sensor or a lidar sensor, the inclusion of ground control points can dramatically increase coordinate accuracy in both data products. A significant amount of time was devoted to adjusting data products and their coordinate reference systems in an attempt to reconcile a 6.5 m disagreement in the x-y plane. The presence of ground control points within the scene would have rapidly corrected this issue.

- The preferred coordinate reference system for data product deliveries needs to be specified in advance. The RIT sUAS lab, the commercial lidar vendor, and the surveying team used three different coordinate reference systems, referencing different geoids for altitude values. In the steps to convert these data products to a common reference system, there is a potential to introduce unnecessary error to the data. This is no fault of the various data sources, as no specific direction was given for preferred coordinate reference system.

- sUAS systems have increased dramatically in their capabilities and use. However, we should remain cognizant of the fact that we are integrating complex sensing and positioning systems on a compact platform. We therefore recommend that adequate system testing and debugging be completed before large research deployments, thereby reducing the risk of data loss or even inaccurate data products.

# Appendix A

# Additional Pre-processing of sUAS Lidar

## A.1 RAW LIDAR FILE REPAIR

### A.1.1 The Issue

It became apparent that a corruption of the time stamps associated with the point returns had occurred during initial alignment of the raw lidar point returns. The misalignment between the lidar time stamps and GPS timestamps was not a standard offset, nor did it form a cyclical pattern. A plot of the of timing stamps, contained within the raw packet capture files generated by the Velodyne VLP-15 lidar sensor, and the correct GPS time for these collections, can be seen in Figure A.1. This sensor supports integration with a 1 Hz synchronization signal accompanied with a NMEA date and time packet, sourced from an external GPS receiver. The lack of correct timing information rendered the task of generating three dimensional point clouds impossible for select sites, as there was no way to synchronize GPS positions, IMU data and lidar return data.

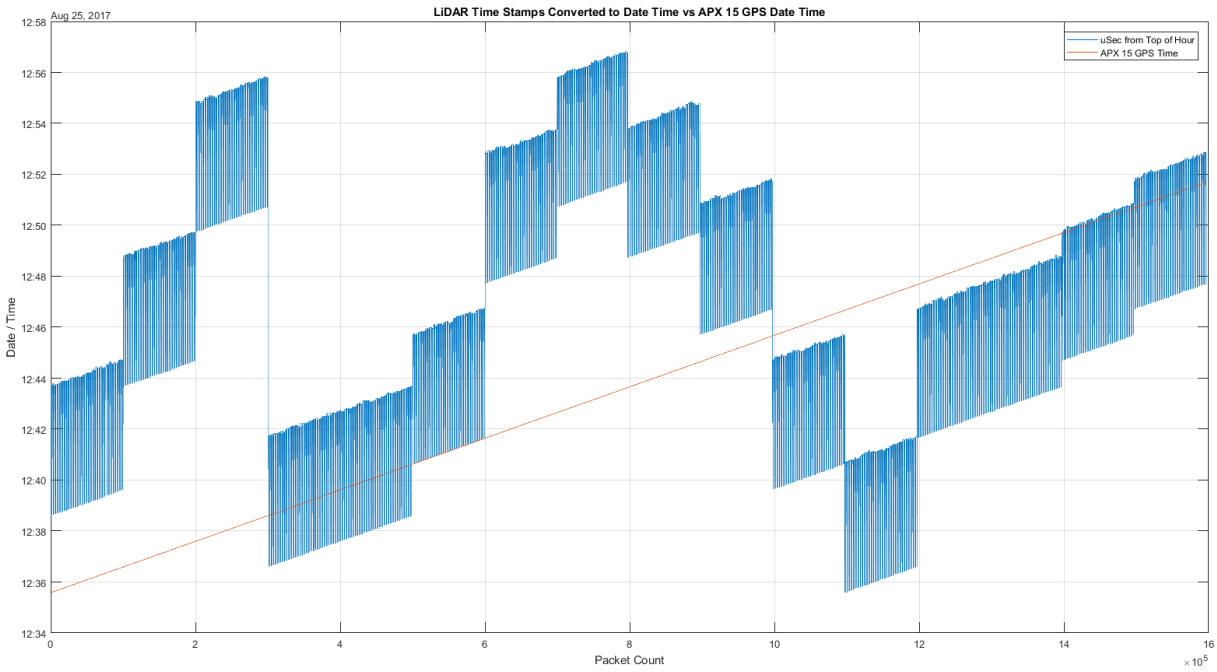


Figure A.1. A depiction of the timing signals seen in the lidar data packets and the correct time stamps, as reported by the GPS receiver log file. The blue lines are the timestamp for each data packet; the red line is the correct time as reported by the GPS receiver. Times are measured from the top of each hour.

### A.2.2 The Repair

A repair was implemented in Matlab, initially developed my Mr. Blair Simon (Headwall Photonics, Bolton, Massachusetts). Mr. Simon's repair code leverages the propagation of internal timing signals of the Nano FPGA, which distributes Unix timestamps to the various peripherals. These time stamps are stored in a GPS log file and a lidar packet index file. The structure of communication between this FPGA and the log files can be seen in Figure A.2; this figure is sourced from a status update given by Mr. Simon during development of the repair code. The information contained within the lidar index file provides Unix timestamps at a coarse sampling rate, with a time stamp write-out sequence approximately once every 100 packets of lidar data. These Unix timestamps can be matched with GPS time stamps entries occurring at the same Unix timestamp to find the true GPS time associated with the specified lidar packet. A linear interpolation of GPS time values are then computed between each time value found for packets in the index file, in order to associate a GPS time with every lidar data packet. If the sampling rate was not constant between index points, an error will be induced by the linear interpolation. These errors were seen as noise in the generated point clouds.

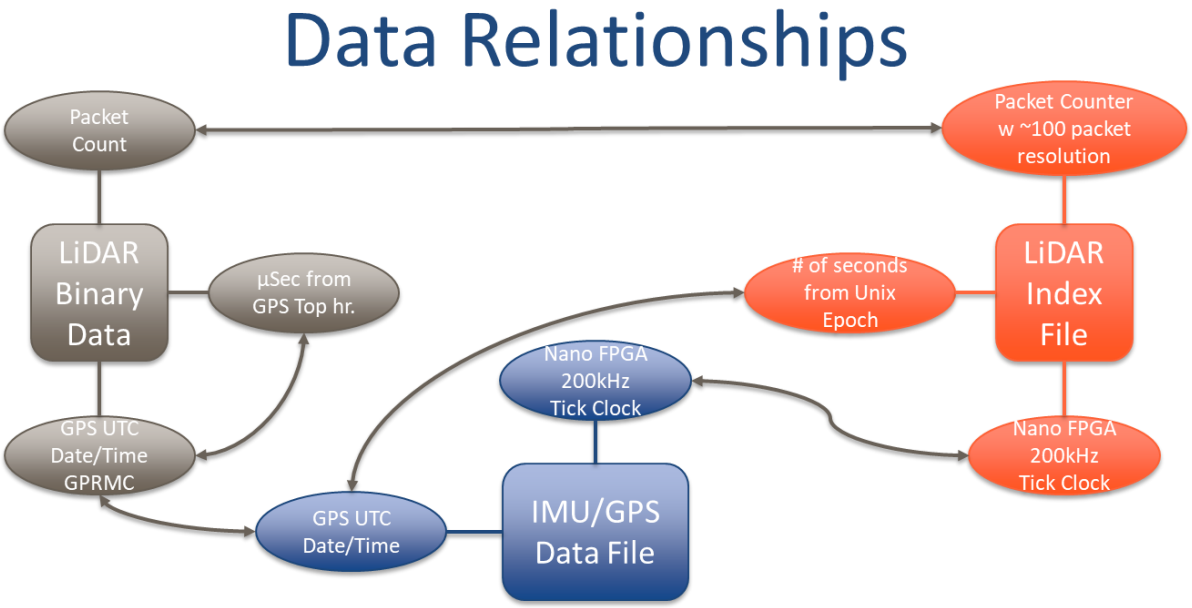


Figure A.2. Flow diagram of timing controls within the MX-1 sUAS.

### A.2.3 Root Cause & Impacts

A mistake in the wiring of the communication signals between the GPS receiver and VLP-16 was determined to be the root cause of this issue. During installation of the communications lines, the technician wired transmitter-to-transmitter and receiver-to-receiver, rather than transmitter-to-receiver. This mistake, coupled with a failure by the UAS Research Lab to conduct any operational tests that included data quality checks, led to a corruption of lidar data for six months of research and up to three separate research projects. In the context of the research presented in this thesis, these mistakes resulted in a seven month delay in delivery of sUAS lidar data and led to a loss of seven flights' worth of data, or 27% of the total data collected.

# Bibliography


[1] K. von Gadow and B. Bredenkamp, *Forest Management*. Academica, 1992.

[2] J. E. Means, S. A. Acker, B. J. Fitt, M. Renslow, L. Emerson, and C. J. H. Abstract, "Predicting Forest Stand Characteristics with Airborne Scanning Lidar," *Photogramm. Eng. Remote Sens.*, vol. 66, no. 11, pp. 1367–1371, 2000.

[3] S. Hummel, A. T. Hudak, E. H. Uebler, M. J. Falkowski, and K. A. Megown, "A Comparison of Accuracy and Cost of LiDAR versus Stand Exam Data for Landscape Management on the Malheur National Forest," *J. For.*, vol. 109, no. August, pp. 267–273, 2011.

[4] B. N. I. Eskelson, H. Temesgen, V. Lemay, T. M. Barrett, N. L. Crookston, and A. T. Hudak, "The roles of nearest neighbor methods in imputing missing data in forest inventory and monitoring databases," *Scand. J. For. Res. 24 235-246.*, pp. 235–246, 2009.

[5] M. L. Imhoff, "Radar backscatter and biomass saturation: ramifications for global biomass inventory," *IEEE Trans. Geosci. Remote Sens.*, vol. 33, no. 2, pp. 511–518, 1995.

[6] R. and S. E. F. Waring, R., Way, J., Hunt Jr., R. Morrissey, L, Ranson, K.J., Weishampel, J.F., Oren, "Imaging Radar for Ecosystcm Studies," *Bioscience*, vol. 45, no. 10, pp. 715–723, 1995.

[7] M. K. Steininger, "Satellite estimation of tropical secondary forest above-ground biomass: Data from Brazil and Bolivia," *Int. J. Remote Sens.*, vol. 21, no. 6–7, pp. 1139–1157, Jan. 2000.

[8] G. M. Foody, G. Palubinskas, R. M. Lucas, P. J. Curran, and M. Honzak, "Identifying terrestrial carbon sinks: Classification of successional stages in regenerating tropical forest from Landsat TM data," *Remote Sens. Environ.*, vol. 55, no. 3, pp. 205–216, Mar. 1996.

[9] P. J. Curran, G. M. Foody, R. M. Lucas, M. Honzak, and J. Grace, "carbon balance of tropical forests: from the local to the regional scale," *Scaling-up from cell to Landsc.*, 1997.

[10] E. F. Moran and E. Brondizio, "Integrating Amazonian vegetation, land-use, and satellite data," *Bioscience*, vol. 44, no. 5, pp. 329–343, 1994.

[11] S. G. Tesfamichael, F. Ahmed, J. A. N. van Aardt, and F. Blakeway, "A semi-variogram approach for estimating stems per hectare in Eucalyptus grandis plantations using discrete-return lidar height data," *For. Ecol. Manage.*, vol. 258, no. 7, pp. 1188–1199, 2009.

[12] S. G. Tesfamichael, J. A. N. van Aardt, and F. Ahmed, "Estimating plot-level tree height and volume of eucalyptus grandis plantations using small-footprint, discrete return lidar data," *Prog. Phys. Geogr.*, vol. 34, no. 4, pp. 515–540, 2010.

[13] J. a N. van Aardt, R. H. Wynne, and J. a Scrivani, "Lidar-based Mapping of Forest Volume and Biomass by Taxonomic Group Using Structurally Homogenous Segments," *Photogramm. Eng. Remote Sens.*, vol. 74, no. 8, pp. 1033–1044, 2008.

[14] J. A. N. Van Aardt *et al.*, "Forest volume and biomass estimation using small-footprint lidar-distributional parameters on a per-segment basis," *For. Sci.*, vol. 52, no. 6, pp. 636–649, 2006.

[15] L. T. Ene, E. Næsset, T. Gobakken, O. M. Bollandsås, E. W. Mauya, and E. Zahabu, "Large-scale estimation of change in aboveground biomass in miombo woodlands using airborne laser scanning and national forest inventory data," *Remote Sens. Environ.*, vol. 188, pp. 106–117, Jan. 2017.

[16] Montréal Process, "Criteria and Indicators for the Conservation and Sustainable Management of Temperate and Boreal Forests (5th Edition)," 2015.

[17] R. J. Keenan, G. A. Reams, F. Achard, J. V. de Freitas, A. Grainger, and E. Lindquist, "Dynamics of global forest area: Results from the FAO Global Forest Resources Assessment 2015," *For. Ecol. Manage.*, vol. 352, pp. 9–20, Sep. 2015.

[18] M. McClelland, J. van Aardt, and D. S. Hale, "A comparison of manned and unmanned aerial Lidar systems in the context of sustainable forest management," in *Autonomous Air and Ground Sensing Systems for Agricultural Optimization and Phenotyping III*, 2018, vol. 10664, p. 26.

[19] E. P. Baltsavias, "Airborne laser scanning: Basic relations and formulas," *ISPRS J. Photogramm. Remote Sens.*, vol. 54, no. 2–3, pp. 199–214, 1999.

[20] R. McGaughey, "FUSION/LDV: Software for LIDAR Data Analysis and Visualization.," *United States Dep. Agric. For. Serv. Pacific Northwest Res. Stn.*, no. October, p. 211, 2016.

[21] R. Nelson, "How did we get here? An early history of forestry lidar [1]," *Can. J. Remote Sens.*, vol. 39, no. sup1, pp. S6–S17, Jun. 2013.

[22] D. B. Lindenmayer, C. R. Margules, and D. B. Botkin, "Indicators of Biodiversity for Ecologically Sustainable Forest Management," *Conserv. Biol.*, vol. 14, no. 4, pp. 941–950, Aug. 2000.

[23] H. Keith, B. G. Mackey, and D. B. Lindenmayer, "Re-evaluation of forest biomass carbon stocks and lessons from the world's most carbon-dense forests.," *Proc. Natl. Acad. Sci. U. S. A.*, vol. 106, no. 28, pp. 11635–40, Jul. 2009.

[24] A. Jaakkola, A. Kukko, X. Yu, H. Kaartinen, M. Lehtomäki, and Y. Lin, "A low-cost multi-sensoral mobile mapping system and its feasibility for tree measurements," *ISPRS J. Photogramm. Remote Sens.*, vol. 65, no. 6, pp. 514–522, Nov. 2010.

[25] L. Wallace, A. Lucieer, C. Watson, and D. Turner, "Development of a UAV-LiDAR system with application to forest inventory," *Remote Sens.*, vol. 4, no. 6, pp. 1519–1543, 2012.

[26] FAA, “Advisory Circular - sUAS Part 017,” *Area*, no. January, pp. 1–4, 2005.

[27] L. Wallace, A. Lucieer, and C. S. Watson, “Evaluating tree detection and segmentation routines on very high resolution UAV LiDAR ata,” *IEEE Trans. Geosci. Remote Sens.*, vol. 52, no. 12, pp. 7619–7628, Dec. 2014.

[28] L. Wallace, R. Musk, and A. Lucieer, “An Assessment of the Repeatability of Automatic Forest Inventory Metrics Derived From UAV-Borne Laser Scanning Data,” *IEEE Trans. Geosci. Remote Sens.*, vol. 52, no. 11, pp. 7160–7169, Nov. 2014.

[29] S. Puliti, L. T. Ene, T. Gobakken, and E. Næsset, “Use of partial-coverage UAV data in sampling for large scale forest inventories,” *Remote Sens. Environ.*, vol. 194, pp. 115–126, Jun. 2017.

[30] Y. Lin, J. Hyyppä, and A. Jaakkola, “Mini-UAV-borne LIDAR for fine-scale mapping,” *IEEE Geosci. Remote Sens. Lett.*, vol. 8, no. 3, pp. 426–430, 2011.

[31] A. Lucieer, D. Turner, D. H. King, and S. A. Robinson, “Using an Unmanned Aerial Vehicle (UAV) to capture micro-topography of Antarctic moss beds,” *Int. J. Appl. Earth Obs. Geoinf.*, vol. 27, pp. 53–62, Apr. 2014.

[32] D. Turner, A. Lucieer, and L. Wallace, “Direct georeferencing of ultrahigh-resolution UAV imagery,” *IEEE Trans. Geosci. Remote Sens.*, vol. 52, no. 5, pp. 2738–2745, May 2014.

[33] I. Colomina and P. Molina, “Unmanned aerial systems for photogrammetry and remote sensing: A review,” *ISPRS J. Photogramm. Remote Sens.*, vol. 92, pp. 79–97, Jun. 2014.

[34] J. P. Dandois and E. C. Ellis, “High spatial resolution three-dimensional mapping of vegetation spectral dynamics using computer vision,” *Remote Sens. Environ.*, vol. 136, pp. 259–276, Sep. 2013.

[35] J. Lisein, M. Pierrot-Deseilligny, S. Bonnet, and P. Lejeune, “A Photogrammetric Workflow for the Creation of a Forest Canopy Height Model from Small Unmanned Aerial System Imagery,” *Forests*, vol. 4, no. 4, pp. 922–944, Nov. 2013.

[36] L. Wallace, A. Lucieer, Z. Malenovský, D. Turner, and P. Vopěnka, “Assessment of Forest Structure Using Two UAV Techniques: A Comparison of Airborne Laser Scanning and Structure from Motion (SfM) Point Clouds,” *Forests*, vol. 7, no. 12, p. 62, Mar. 2016.

[37] T. Ota *et al.*, “Aboveground Biomass Estimation Using Structure from Motion Approach with Aerial Photographs in a Seasonal Tropical Forest,” *Forests*, vol. 6, no. 12, pp. 3882–3898, Oct. 2015.

[38] H. Qin, C. Wang, X. Xi, J. Tian, and G. Zhou, “Simulating the Effects of the Airborne Lidar Scanning Angle, Flying Altitude, and Pulse Density for Forest Foliage Profile Retrieval,” *Appl. Sci.*, vol. 7, no. 7, p. 712, 2017.

[39] J. S. Evans and A. T. Hudak, “A multiscale curvature algorithm for classifying discrete return LiDAR in forested environments,” *IEEE Trans. Geosci. Remote Sens.*, vol. 45, no. 4, pp. 1029–1038, 2007.

[40] L. O. Wallace, A. Lucieer, and C. S. Watson, “Assessing the Feasibility of Uav-Based Lidar for High Resolution Forest Change Detection,” *ISPRS - Int. Arch. Photogramm. Remote Sens. Spat. Inf. Sci.*, vol. XXXIX-B7, no. September, pp. 499–504, 2012.

[41] P. Axelsson, “DEM Generation from Laser Scanner Data Using adaptive TIN Models,” *Int. Arch. Photogramm. Remote Sens.*, vol. 23, no. B4, pp. 110–117, 2000.

[42] M. Isenburg, “LAStools - efficient LiDAR processing software (version 180520, academic license).” rapidlasso GmbH, 2018.

[43] K. Kraus and N. Pfeifer, “Determination of terrain models in wooded areas with airborne laser scanner data,” *ISPRS J. Photogramm. Remote Sens.*, vol. 53, no. 4, pp. 193–203, Aug. 1998.

[44] G. L. Heritage, D. J. Milan, A. R. G. Large, and I. C. Fuller, “Influence of survey strategy and interpolation model on DEM quality,” *Geomorphology*, vol. 112, no. 3–4, pp. 334–344, Nov. 2009.

[45] “About Us | Rainforest Alliance.” [Online]. Available: https://www.rainforest-alliance.org/about. [Accessed: 08-Mar-2018].

[46] “The Rainforest Alliance Announces New Project Focused on Sustainable Forestry in Southeast Region of United States | Rainforest Alliance.” [Online]. Available: https://www.rainforest-alliance.org/press-releases/southeast-sustainable-forestry-announcement. [Accessed: 08-Mar-2018].

[47] “2018 Federal General Wage Schedule.” [Online]. Available: https://www.opm.gov/policy-data-oversight/pay-leave/salaries-wages/salary-tables/pdf/2018/GS.pdf. [Accessed: 09-Mar-2018].

[48] Q. QGIS Development Team, “QGIS Geographic Information System.” Open Source Geospatial Foundation, 2017.

[49] S. G. Zolkos, S. J. Goetz, and R. Dubayah, “A meta-analysis of terrestrial aboveground biomass estimation using lidar remote sensing,” *Remote Sens. Environ.*, vol. 128, pp. 289–298, Jan. 2013.

[50] “CPI Inflation Calculator.” [Online]. Available: https://data.bls.gov/cgi-bin/cpicalc.pl. [Accessed: 10-Mar-2018].

[51] G. B. Bonan, “Forests and climate change: forcings, feedbacks, and the climate benefits of forests.,” *Science*, vol. 320, no. 5882, pp. 1444–9, Jun. 2008.

[52] K. Zhao and R. B. Jackson, “Biophysical forcings of land-use changes from potential forestry activities in North America,” *Ecol. Monogr.*, vol. 84, no. 2, pp. 329–353, May 2014.

[53] M. A. Wulder, C. W. Bater, N. C. Coops, T. Hilker, and J. C. White, “The role of LiDAR in sustainable forest management,” *— For. Chron.*, vol. 84, no. 6, 2008.

[54] J. Hyyppä, M. Holopainen, and H. Olsson, “Laser Scanning in Forests,” *Remote Sens.*, vol. 4, no. 10, pp. 2919–2922, Sep. 2012.

[55] C. McElhinny, P. Gibbons, C. Brack, and J. Bauhus, "Forest and woodland stand structural complexity: Its definition and measurement," *For. Ecol. Manage.*, vol. 218, no. 1–3, pp. 1–24, Oct. 2005.

[56] M. Messinger, G. P. Asner, and M. Silman, "Rapid assessments of amazon forest structure and biomass using small unmanned aerial systems," *Remote Sens.*, vol. 8, no. 8, pp. 1–15, 2016.

[57] G. Jozkow, P. Wieczorek, M. Karpina, A. Walicka, and A. Borkowski, "PERFORMANCE EVALUATION OF sUAS EQUIPPED WITH VELODYNE HDL-32E LiDAR SENSOR," 2017.

[58] K. Zhao, S. Popescu, and R. Nelson, "Lidar remote sensing of forest biomass: A scale-invariant estimation approach using airborne lasers," *Remote Sens. Environ.*, vol. 113, no. 1, pp. 182–196, Jan. 2009.

[59] E. Næsset and K.-O. Bjerknes, "Estimating tree heights and number of stems in young forest stands using airborne laser scanner data," *Remote Sens. Environ.*, vol. 78, no. 3, pp. 328–340, Dec. 2001.

[60] J. E. Means *et al.*, "Use of Large-Footprint Scanning Airborne Lidar To Estimate Forest Stand Characteristics in the Western Cascades of Oregon," *Remote Sens. Environ.*, vol. 67, no. 3, pp. 298–308, Mar. 1999.

[61] M. A. Lefsky, W. B. Cohen, S. A. Acker, G. G. Parker, T. A. Spies, and D. Harding, "Lidar Remote Sensing of the Canopy Structure and Biophysical Properties of Douglas-Fir Western Hemlock Forests," *Remote Sens. Environ.*, vol. 70, no. 3, pp. 339–361, Dec. 1999.

[62] R. Nelson, A. Short, and M. Valenti, *Measuring biomass and carbon in Delaware using an airborne profiling LIDAR*, vol. 19, no. 6. 2004.

[63] K. Zhao, J. C. Suarez, M. Garcia, T. Hu, C. Wang, and A. Londo, "Utility of multitemporal lidar for forest and carbon monitoring: Tree growth, biomass dynamics, and carbon flux," *Remote Sens. Environ.*, vol. 204, pp. 883–897, Jan. 2018.

[64] "AgiSoft PhotoScan Professional (Version 1.2.6)." 2016.

[65] G. Verhoeven, "Taking computer vision aloft - archaeological three-dimensional reconstructions from aerial photographs with photoscan," *Archaeol. Prospect.*, vol. 18, no. 1, pp. 67–73, Jan. 2011.

[66] S. Englhart, J. Jubanski, and F. Siegert, "Quantifying Dynamics in Tropical Peat Swamp Forest Biomass with Multi-Temporal LiDAR Datasets," *Remote Sens.*, vol. 5, no. 5, pp. 2368–2388, May 2013.

[67] S. Goetz and R. Dubayah, "Advances in remote sensing technology and implications for measuring and monitoring forest carbon stocks and change," *Carbon Manag.*, vol. 2, no. 3, pp. 231–244, Jun. 2011.

[68] J. B. Drake *et al.*, "Estimation of tropical forest structural characteristics using large-footprint lidar," *Remote Sens. Environ.*, vol. 79, no. 2–3, pp. 305–319, Feb. 2002.

[69] J. B. Drake, R. O. Dubayah, R. G. Knox, D. B. Clark, and J. . Blair, "Sensitivity of large-footprint lidar to canopy structure and biomass in a neotropical rainforest," *Remote Sens. Environ.*, vol. 81, no. 2–3, pp. 378–392, Aug. 2002.

[70] S. Magnussen, E. Næsset, G. Kändler, P. Adler, J. P. Renaud, and T. Gobakken, "A functional regression model for inventories supported by aerial laser scanner data or photogrammetric point clouds," *Remote Sens. Environ.*, vol. 184, pp. 496–505, Oct. 2016.

[71] Mathworks, "Matlab." The MathWorks, Inc., Natick, MA, 2016.

[72] X. Yu, J. Hyyppä, H. Kaartinen, and M. Maltamo, "Automatic detection of harvested trees and determination of forest growth using airborne laser scanning," *Remote Sens. Environ.*, vol. 90, no. 4, pp. 451–462, Apr. 2004.

[73] J. L. Lovell, D. L. B. Jupp, D. S. Culvenor, and N. C. Coops, "Using airborne and ground-based ranging lidar to measure canopy structure in Australian forests," *Can. J. Remote Sens.*, vol. 29, no. 5, pp. 607–622, Oct. 2003.

[74] R. Kohavi, "A Study of Cross-Validation and Bootstrap for Accuracy Estimation and Model Selection," *Learning*, vol. 14, no. March 2001, pp. 1137–1143, 2001.

[75] G. Shao, G. Shao, J. Gallion, M. R. Saunders, J. R. Frankenberger, and S. Fei, "Improving Lidar-based aboveground biomass estimation of temperate hardwood forests with varying site productivity," *Remote Sens. Environ.*, vol. 204, pp. 872–882, Jan. 2018.

[76] M. Sumnall, A. Peduzzi, T. R. Fox, R. H. Wynne, and V. A. Thomas, "Analysis of a lidar voxel-derived vertical profile at the plot and individual tree scales for the estimation of forest canopy layer characteristics," *Int. J. Remote Sens.*, vol. 37, no. 11, pp. 2653–2681, Jun. 2016.

[77] A. Shmilovici, "Support Vector Machines," in *Data Mining and Knowledge Discovery Handbook*, O. Maimon and L. Rokach, Eds. Boston, MA: Springer US, 2010, pp. 231–247.

[78] D. A. Coomes *et al.*, "Area-based vs tree-centric approaches to mapping forest carbon in Southeast Asian forests from airborne laser scanning data," *Remote Sens. Environ.*, vol. 194, pp. 77–88, Jun. 2017.